Advanced Energy Harvesting Vibration Absorbers Using Inertial Amplifiers

Sudip Chowdhury, Ph.D.[1]; Sondipon Adhikari, Ph.D.[2]; and Arnab Banerjee, Ph.D.[3]

Abstract: Conventional dynamic vibration absorbers (DVAs) face challenges in achieving optimal vibration suppression and efficient energy harvesting due to design limitations and the absence of exact closed-form analytical solutions. To address this, an inertial amplifier energy harvesting dynamic vibration absorber (IAEHDVA) is introduced in this paper. Using inertial amplifiers and piezoelectric stacks, it combines vibration-mitigation and energy harvesting capabilities. Advanced H_2 and H_∞ optimization methods are employed to derive closed-form analytical solutions for optimal tuning and damping ratios. The results demonstrate that the IAEHDVA outperforms conventional and inerter-based absorbers, achieving up to 64.23% greater vibration suppression and 98.85% higher energy harvesting efficiency. This novel absorber provides a sustainable and optimized solution for vibration control and energy harvesting. **DOI: 10.1061/AJRUA6.RUENG-1529.** © *2025 American Society of Civil Engineers.*

Practical Applications: The IAEHDVA demonstrates considerable potential for practical implementation across various engineering domains. Its ability to simultaneously suppress vibrations and harvest energy makes it highly suitable for infrastructure requiring sustainable solutions. For instance, in civil engineering, the IAEHDVA can enhance the resilience of buildings, bridges, skyscrapers, and offshore platforms by mitigating the effects of wind and seismic excitations, thereby extending their operational life spans. The integration of piezoelectric stacks enables the device to convert mechanical vibrations into electrical energy, creating a self-sustained system that reduces reliance on external power sources. This feature is particularly beneficial in remote or off-grid locations where energy supply can be intermittent or unavailable. Furthermore, the IAEHDVA's compact design, facilitated by inertial amplifiers, addresses challenges related to space constraints and weight, making it an ideal choice for modern lightweight structures and renewable energy systems, such as offshore wind turbines. By improving vibration suppression and energy efficiency, the IAEHDVA supports the global transition to sustainable infrastructure and aligns with net-zero carbon emission goals.

Author keywords: Inertial amplifier energy harvesting dynamic vibration absorber (IAEHDVA); Piezoelectric stacks; H_2 and H_∞ optimization methods; Efficient energy harvesting; Vibration suppression.

Introduction

Dynamic vibration absorbers (DVAs) are devices used in engineering applications to reduce or eliminate vibrations in mechanical systems (Ormondroyd and Den Hartog 1928). Their inherent frequency is engineered to be almost identical with the frequency of undesired vibrations in the applied system (Su et al. 2024). These devices are often passive systems, running without the need for an external power supply (Chowdhury and Banerjee 2024). They are used to reduce vibrations caused by wind in bridges and tall structures, increase stability in machines, and manage vibrations in airplanes (Yu et al. 2024). Despite their efficacy, conventional tuned mass dampers (TMDs) encounter numerous limitations (Huang et al. 2018), such as a narrow frequency bandwidth, difficulties in accommodating diverse dynamic loads, and challenges in improving vibration attenuation capacity due to the augmented static mass of individual dampers or the collective weight of multiple dampers (Huo et al. 2023). The conventional TMDs correspond to DVAs. Therefore, an effective mass amplification device needs to incorporate with the conventional dampers.

The vibration attenuation capacity of TMDs is further tried to improve by incorporating electrostatic mechanisms, piezoelectric materials, and electromagnetic induction (Caracoglia 2024) inside their core material. Energy harvesting DVAs are designed to capture and transform mechanical oscillations or vibrations into electrical energy that can be used (Ali and Adhikari 2013). These devices produce electricity from ambient mechanical energy and aid in reducing vibrations in a system. They are especially important in situations where there are vibrations, such as in equipment, buildings, or wearable technology (Madhav and Ali 2016). It has provided combined vibration mitigation and energy harvesting capabilities to the TMDs.

The piezoelectric materials inside the energy harvesting dynamic vibration absorbers (EHDVAs) react to mechanical stress or vibrations by producing an electric charge (Ali et al. 2011). DVA constructions often include piezoelectric components (Adhikari and Banerjee 2022; Kang et al. 2024), which enable them to transform the mechanical energy that is absorbed into electrical energy (Brennan et al. 2014). A magnet is moved within a coil to create an electrical current through the process of electromagnetic induction (Chen et al. 2023). By collecting vibrations and powering sensors,

[1]Research Associate, James Watt School of Engineering, Univ. of Glasgow, Glasgow, Scotland G12 8QQ, UK (corresponding author). ORCID: https://orcid.org/0000-0001-6218-4843. Email: Sudip.Chowdhury@glasgow.ac.uk

[2]Professor of Engineering Mechanics, James Watt School of Engineering, Univ. of Glasgow, Glasgow, Scotland G12 8QQ, UK. Email: Sondipon.Adhikari@glasgow.ac.uk

[3]Associate Professor, Civil Engineering Dept., Indian Institute of Technology Delhi, New Delhi 110016, India. Email: abanerjee@iitd.ac.in

Note. This manuscript was submitted on October 3, 2024; approved on February 14, 2025; published online on May 20, 2025. Discussion period open until October 20, 2025; separate discussions must be submitted for individual papers. This paper is part of the ***ASCE-ASME Journal of Risk and Uncertainty in Engineering Systems, Part A: Civil Engineering***, © ASCE, ISSN 2376-7642.

energy harvesting DVAs can be used in civil engineering to monitor the integrity and health of structures (dos Santos 2023). Wearable devices can benefit from energy harvesting DVAs as they can capture the wearer's motions and use them to generate electrical power for the gadget (Kakou and Barry 2021). Efficient DVAs with integrated energy harvesting systems need to be carefully tuned to match the vibrations of the surrounding environment in terms of both frequency and amplitude (Loong et al. 2023).

For practical applications, achieving great efficiency in energy conversion and absorption is essential (Su et al. 2023). Dynamic vibration absorbers that incorporate energy harvesting become more efficient and eco-friendly due to the development of self-sufficient, sustainable systems (Raj and Santhosh 2019). Overall, EHDVAs offer dual functionalities of vibration mitigation and energy harvesting, but they come with several drawbacks that limit their overall performance. A notable disadvantage is their diminished potential for vibration reduction because the incorporation of energy harvesting components often undermines the absorber's core purpose of vibration control (Wang et al. 2019). The added complexity from energy conversion mechanisms, such as piezoelectric transducers, can reduce the absorber's ability to effectively suppress structural vibrations. Additionally, their energy conversion efficiency remains limited, especially under variable excitations, due to suboptimal tuning. Design and optimization issues emerge from the need for exact calibration to align with certain vibration frequencies (Chowdhury et al. 2024d). The incorporation of energy harvesting devices increases weight and space demands, possibly influencing the dynamic response of the host building. EHDVAs often face challenges in maintaining optimal performance due to difficulties in effectively adapting to diverse and varying dynamic loads.

Advancement in TMD design aims to overcome these limits through the integration of novel mechanisms and optimization methodologies (Chowdhury and Debbarma 2025). For example, H_2 optimization is used to ascertain the optimal tuning frequency and damping ratios of TMDs (Chowdhury and Adhikari 2024) based on the mean-square dynamic responses to random excitations (Roberts and Spanos 2003). Likewise, H_∞ optimization is used to extract these parameters from the dynamic responses of TMD-controlled devices exposed to harmonic excitations (Chowdhury et al. 2024c). Although these optimization strategies can improve TMD performance, issues of spatial limitations and weight are still unaddressed.

Recently, Smith (2002) has introduced inerters. This is an effective mass amplification device which improve vibration attenuation performance by inserting them both horizontally and vertically into the absorber's core). These inerters are used in mechanical structures, civil engineering constructions, and tuned mass dampers to lessen dynamic reactions during earthquakes and storms (Chen and Hu 2019). Inerters are also incorporated with EHDVAs to enhance their performances. However, that is not significantly higher than conventional absorbers, making it difficult to find optimal design (Giaralis 2021). In addition, the energy harvesting capacity is also lower. Therefore, inerters fail to provide significant enhancement in vibration attenuation and energy harvesting capacity to the TMD and EHDVA.

An alternative effective mass amplification device is needed to address these limitations. Inertial amplifiers (Yilmaz et al. 2007), as an effective mass amplification device (Frandsen et al. 2016), are placed in the cores of the conventional dampers to improve their dynamic attenuation performance (Chowdhury and Adhikari 2024). Negative stiffness devices, extensively researched in mechanical metamaterials, also enhance the vibration attenuation capability of conventional absorbers (Shen et al. 2017). Hybrid metamaterial conceptualization, such as the passive fusion of inertial amplifiers and negative stiffness devices, benefits the improvement of vibration attenuation performance for conventional passive dampers (Chowdhury et al. 2024b). However, these approaches did not suppress all the drawbacks of conventional vibration absorbers (Rajarathinam and Ali 2021).

Inertial amplifiers can enhance the effective mass of vibration absorbers (Chowdhury et al. 2023) and address many limitations of conventional designs (Chowdhury et al. 2024a). However, inertial amplifier tuned mass dampers lack integrated energy harvesting capabilities, limiting their potential for renewable energy applications. Currently, there are no state-of-the-art inertially amplified energy harvesting dynamic vibration absorbers and corresponding optimal closed-form solutions. This significant research gap highlights the absence of advanced designs and analytical frameworks addressing these systems.

To address this research gap, the paper introduces an inertially amplified energy harvesting dynamic vibration absorber (IAEHDVA). This innovative absorber integrates piezoelectric stacks to convert mechanical vibrations into electrical energy, enabling both effective vibration control and sustainable energy generation. Advanced H_2 and H_∞ optimization algorithms are employed to derive closed-form analytical solutions for optimal frequency and damping ratios, filling a critical void in the existing literature. The vibration reduction and energy harvesting capacities of the proposed absorbers are systematically compared with those of conventional absorbers, demonstrating their superior performance.

Inertial Amplifier Energy Harvesting Dynamic Vibration Absorber

TMDs are extensively employed to mitigate dynamic responses in structural systems, particularly when installed at the apex of tall structures. Traditional approaches to enhancing the vibration attenuation performance of TMDs often involve increasing their static mass. However, this strategy introduces challenges such as higher material demands and the risk of damage to the damper's base layer under high-amplitude vibrations. To overcome these limitations, an advanced TMD design integrating a piezoelectric element and an effective mass amplification mechanism embedded within the damper's core material is introduced in this paper. The piezoelectric component facilitates the conversion of mechanical energy into electrical energy, enabling energy harvesting and improving system efficiency. Concurrently, the effective mass amplification mechanism dissipates additional energy, enhancing the damper's overall attenuation capabilities. This hybrid configuration reduces reliance on excessive static mass while ensuring superior vibration control. Moreover, the dual functionality of energy harvesting and enhanced damping provides a sustainable, high-performance solution for structures subjected to both harmonic and random excitations, advancing resilient and energy-efficient structural designs.

System Formulation and Equations of Motion

The IAEHDVA is attached at the top of a single-degree-of-freedom (SDOF) system. An external force P is applied to the mass m of the SDOF system, which is shown in Fig. 1. As a result, a small deflection occurs at the SDOF system and the absorber, i.e., v_s and v_u. In addition, the effective mass of the absorbers has been increased. Simultaneously, other system properties, such as stiffness and damping have also been changed. The effective mass, stiffness, and damping of IAEHDVA are derived as m_u, k_u, and c_u, where $m_u = m_v + 0.5m_z\Theta$, $\Theta = [1 + (1/\tan^2\phi)]$, $k_u = m_u\nu^2$, and $c_u =$

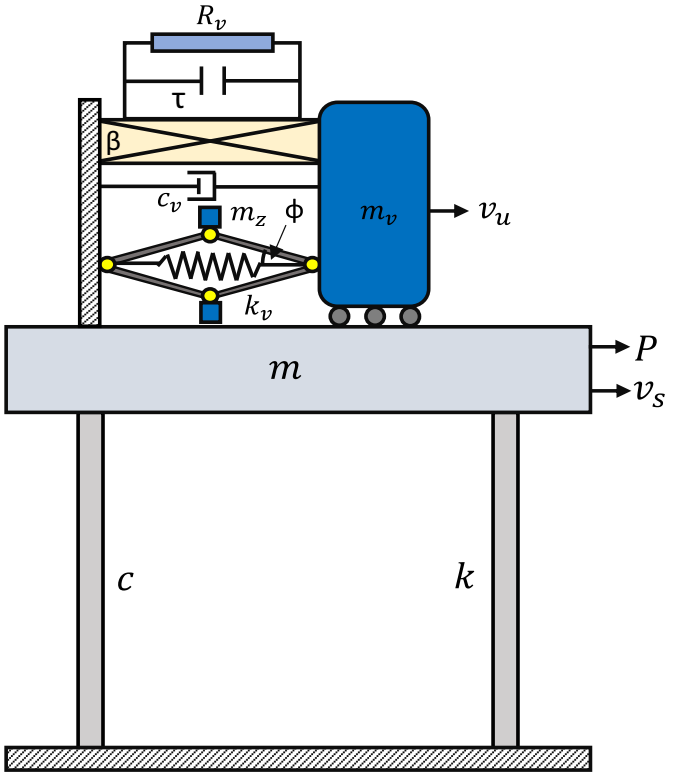

Fig. 1. Single-degree-of-freedom system with attached inertial amplifier energy harvesting dynamic vibration absorber.

$2m_u\xi\nu$. The static mass, stiffness, and damping, i.e., m_v, k_v, and c_v, of the absorber are converted to m_u, k_u, and c_u. Here, m_z defines the amplifier's mass, ϕ defines the amplifier/inertial angle, and ξ and ν define the damping ratio and natural frequency of the IAEHDVA.

Next, $\Upsilon = m_u/m$ defines the effective mass ratio of the absorber; ζ and ε define the damping ratio and natural frequency of the SDOF system. $\Upsilon_v = m_v/m$ defines the absorber mass ratio, and $\chi = \nu/\varepsilon$ defines the frequency ratio of the absorber. $\Upsilon_z = m_z/m$ defines the amplifier mass ratio. The stiffness and damping of the SDOF system is considered as $k = m\varepsilon^2$ and $c = 2m\zeta\varepsilon$. The energy harvesting characteristic for the absorber is produced through the inside attached piezoelectric stack coupling the electrical and mechanical parts of the harvester of β and the electrical capacitance and resistance of τ and R_v. A voltage v is generated over the load resistor.

Newton's second law is employed to derive the governing equations of motion of the controlled SDOF system. Hence, the equation of motion for controlled SDOF is obtained as follows:

$$m\ddot{v}_s + c\dot{v}_s + kv_s - k_u(v_u - v_s) - c_u(\dot{v}_u - \dot{v}_s) = P \tag{1}$$

The electromechanical coupling and mechanical force are both proportional to the voltage across the piezoceramic membrane. The equation of motion for the absorber is obtained as follows:

$$m_u\ddot{v}_u + c_u(\dot{v}_u - \dot{v}_s) + k_u(v_u - v_s) - \beta v = 0 \tag{2}$$

The equation of motion for the piezoelectric stack is obtained as follows:

$$\tau\dot{v} + \frac{v}{R_v} + \beta\dot{v}_u = 0 \tag{3}$$

Eq. (3) is derived from the electrical circuit, in which the voltage across the load resistance is generated by mechanical strain via electromechanical coupling and the piezoceramic τ capacitance. The steady-state solutions are considered as $v_s = V_s e^{i\omega t}$, $v_u = V_u e^{i\omega t}$, $v = Ve^{i\omega t}$, and $P = P_o e^{i\omega t}$. Applying these steady-state solutions to Eqs. (1)–(3), the frequency response function has been derived and expressed as follows:

$$\begin{bmatrix} A_{11} & -2\,i\eta\xi\Upsilon\chi - \Upsilon\chi^2 & 0 \\ -2\,i\eta\xi\chi - \chi^2 & -\eta^2 + 2\,i\eta\xi\chi + \chi^2 & -\dfrac{\beta\chi^2}{k_u} \\ 0 & \dfrac{i\eta\beta\delta}{\tau} & i\delta\eta + \chi \end{bmatrix} \begin{Bmatrix} V_s \\ V_u \\ V \end{Bmatrix} = \begin{bmatrix} 1 \\ 0 \\ 0 \end{bmatrix} \left(\frac{P_o}{m\varepsilon^2}\right) \tag{4}$$

$$A_{11} = -\eta^2 + 2\,i\zeta\eta + 2\,i\eta\xi\Upsilon\chi + \Upsilon\chi^2 + 1 \tag{5}$$

where ζ is considered zero (i.e., $\zeta = 0$) to derive the optimal design parameters of the absorber in terms of a closed-form expression using H_2 and H_∞ optimization methods. The dynamic response of the SDOF system is

$$W_s = \left(\frac{V_s}{P_o}\right)k = \frac{-2\chi\delta\eta^2\xi + \chi^3 - \chi\eta^2 + i(\kappa^2\chi^2\eta\delta + \chi^2\delta\eta + 2\chi^2\eta\xi - \delta\eta^3)}{\Lambda} \tag{6}$$

The dynamic response of the absorber is

$$W_u = \left(\frac{V_u}{P_o}\right)k = \frac{-2\chi\eta^2\xi\delta + \chi^3 + i(\chi^2\delta\eta + 2\eta\xi\chi^2)}{\Lambda} \tag{7}$$

The voltage of the piezoelectric stack is

$$W_v = \left(\frac{V}{P_o}\right)k = \frac{-\frac{(i\chi - 2\eta\xi)\chi\beta\eta\delta}{\tau}}{\Lambda} \tag{8}$$

The denominator of Eqs. (6)–(8) is derived as follows:

$$\begin{aligned}\Lambda = {} & \delta q^5 + (2\chi\xi\delta\Upsilon + 2\chi\xi\delta + \chi)q^4 \\ & + (\kappa^2\delta\chi^2 + \Upsilon\delta\chi^2 + 2\Upsilon\chi^2\xi + \chi^2\delta + 2\xi\chi^2 + \delta)q^3 \\ & + (2\chi^3\xi\kappa^2\delta\Upsilon + \chi^3\Upsilon + \chi^3 + 2\chi\xi\delta + \chi)q^2 \\ & + (\kappa^2\Upsilon\delta\chi^4 + \kappa^2\delta\chi^2 + \chi^2\delta + 2\xi\chi^2)q + \chi^3\end{aligned} \tag{9}$$

where $q = i\eta$, where $i = \sqrt{-1}$ defines the imaginary number, and $\eta = \omega/\varepsilon$ defines the excitation frequency ratio. The nondimensional electromechanical coupling coefficient is considered as $\kappa^2 = \beta^2/k_u\tau$. The nondimensional time constant is considered as $\delta = \nu\tau R_v$.

These equations are applied to derive the optimal design parameters for IAEHDVA. Although the steady-state approach was employed for harmonic excitations, the H_2 optimization method explicitly considers random excitations, providing a robust framework for deriving the optimal parameters under stochastic conditions. This approach ensures that the derived solutions account for

the effects of random, nonharmonic disturbances, enhancing their precision and applicability in realistic scenarios.

Derivation of H_2-Optimized Design Parameters

The H_2 optimization method for the novel IAEHDVA focuses on minimizing the variance of the system's response under stochastic excitations, such as white noise. By employing statistical energy principles, the method evaluates the mean-square response of the primary system to derive optimal tuning and damping ratios. This involves solving the dynamic equations of motion to compute the system's frequency response function, where the absorber's design parameters are adjusted to achieve minimal energy amplification in the system. The closed-form expressions for optimal parameters ensure that the absorber effectively suppresses vibrations while maintaining robustness against varying dynamic loads. This optimization framework enhances the absorber's performance by considering both the dynamic coupling effects and the inherent randomness in the excitation.

In the H_2 optimization technique, the damping ratio of the primary structure is considered to be zero, i.e., $\zeta = 0$, to facilitate mathematical derivations and allow for closed-form analytical formulas for the optimal tuning frequency and damping ratio of the damper. This assumption removes the influence of structural dampening, isolating the damper's role in vibration control and guaranteeing accurate and effective optimization parameters. The controlled structure is subjected to white noise excitations, making the H_2 optimization method suitable for this analysis. Eq. (9), representing a fifth-order polynomial, is utilized to derive the variance of the dynamic response of the structure. This variance quantifies the system's energy amplification under stochastic excitations, serving as a key metric for determining the optimal absorber parameters

$$\Sigma^2_{W_s} = \frac{\pi S_0(S_1)}{\Upsilon\chi(S_2)} \tag{10}$$

The closed-form expressions for S_1 and S_2 are provided in the Appendix, where S_0 represents the spectral density, assumed constant across all frequencies. Minimizing the variance of the dynamic response of the primary structure is critical to mitigating vibration-induced effects. Consequently, the optimal design parameters for the absorbers can be determined using Eq. (10). The mathematical framework for this derivation process is outlined in detail to ensure precision and clarity in the optimization procedure

$$\frac{\partial\Sigma^2_{W_s}}{\partial\xi} = 0 \quad \text{and} \quad \frac{\partial\Sigma^2_{W_s}}{\partial\chi} = 0 \tag{11}$$

Eq. (10) is substituted into the first equation of Eq. (11), leading to the derivation of the damping ratio of the absorber

$$\xi = \frac{\begin{array}{c}128\Upsilon\chi^6\delta + 192\Upsilon\chi^4\delta^3 + 64\Upsilon\chi^2\delta^5 + 64\chi^6\delta + 128\chi^4\delta^3 + 64\chi^2\delta^5 - 64\Upsilon^4\chi^8\delta^5\kappa^6 + 64\Upsilon^2\chi^8\delta^7\kappa^6 - 256\Upsilon^3\chi^8\delta^5\kappa^6 + 64\Upsilon\chi^8\delta^7\kappa^6 \\ -256\Upsilon^4\chi^8\delta^5\kappa^4 - 448\Upsilon^2\chi^8\delta^5\kappa^6 - 1{,}024\Upsilon^3\chi^8\delta^5\kappa^4 - 384\Upsilon\chi^8\delta^5\kappa^6 + 64\Upsilon\chi^6\delta^7\kappa^6 - 1{,}472\Upsilon^2\chi^8\delta^5\kappa^4 - 128\Upsilon^2\chi^6\delta^7\kappa^4 - 128\chi^8\delta^5\kappa^6 \\ +64\chi^6\delta^7\kappa^6 - 64\Upsilon^3\chi^8\delta^3\kappa^4 - 64\Upsilon^3\chi^6\delta^5\kappa^4 - 896\Upsilon\chi^8\delta^5\kappa^4 + 128\chi^4\delta^5 - 64\Upsilon\chi^6\delta^7\kappa^4 + 192\Upsilon^4\chi^8\delta^3\kappa^2 - 192\Upsilon^2\chi^8\delta^3\kappa^4 \\ -128\Upsilon^2\chi^6\delta^5\kappa^4 - 192\chi^8\delta^5\kappa^4 + 64\chi^6\delta^7\kappa^4 + 704\Upsilon^3\chi^8\delta^3\kappa^2 + 256\Upsilon^3\chi^6\delta^5\kappa^2 - 192\Upsilon\chi^8\delta^3\kappa^4 - 128\Upsilon\chi^4\delta^7\kappa^4 + 960\Upsilon^2\chi^8\delta^3\kappa^2 \\ +512\Upsilon^2\chi^6\delta^5\kappa^2 + 64\Upsilon^2\chi^4\delta^7\kappa^2 - 64\chi^8\delta^3\kappa^4 + 64\chi^6\delta^5\kappa^4 + 64\chi^2\delta^7 - 128\chi^4\delta^7\kappa^4 + 576\Upsilon\chi^8\delta^3\kappa^2 + 256\Upsilon\chi^6\delta^5\kappa^2 - 64\Upsilon\chi^4\delta^7\kappa^2 \\ -128\Upsilon^2\chi^6\delta^3\kappa^2 + 64\Upsilon^2\chi^4\delta^5\kappa^2 + 128\chi^8\delta^3\kappa^2 - 128\chi^4\delta^7\kappa^2 + 64\Upsilon^3\chi^6\delta^3 - 256\Upsilon\chi^6\delta^3\kappa^2 + 64\chi^6\delta^3 + 64\Upsilon\chi^2\delta^7\kappa^2 + 192\Upsilon^2\chi^6\delta^3 \\ +128\Upsilon^2\chi^4\delta^5 - 128\chi^6\delta^3\kappa^2 - 64\chi^4\delta^5\kappa^2 + 64\chi^2\delta^7\kappa^2 + 192\Upsilon\chi^6\delta^3 + 256\Upsilon\chi^4\delta^5 + 64\Upsilon\chi^2\delta^7 + 64\Upsilon^2\chi^6\delta + 64\Upsilon^2\chi^4\delta^3\end{array}}{S_3} \tag{12}$$

where S_3 has been derived as a function of the system's dynamic parameters, encapsulating the relationships between the absorber's mass ratio, frequency ratio, and damping ratio

$$S_3 = 384(\delta^2\kappa^4(\Upsilon+1)^3\chi^6 + (-\delta^4\kappa^4 + \kappa^2(\Upsilon+2)(\Upsilon+1)\delta^2 - (\Upsilon+1)^2)\chi^4 + 2\delta^2(\delta^2\kappa^2 - \Upsilon - 1)\chi^2 - \delta^4)\delta^2(\Upsilon+1)\chi^2 \tag{13}$$

Next, Eq. (12) is substituted into Eq. (10), resulting in a modified expression for the variance of the dynamic response of the primary structure. This modified variance is then incorporated into the second equation of Eq. (11) to refine the optimization process. Consequently, the optimal frequency of the absorber is derived, ensuring an accurate and efficient design parameter for the system

$$(\chi)_{\text{opt}} = \sqrt{\frac{S_4}{S_5}} \tag{14}$$

The closed-form expressions for S_4 and S_5 are listed in the Appendix.

H_∞ Optimization for IAEHDVA

The H_∞ optimization for the novel IAEHDVA targets minimizing the maximum dynamic response of the system under harmonic excitations, ensuring robust performance against worst-case scenarios. This approach utilizes frequency-domain techniques to identify the absorber's optimal tuning and damping ratios by solving mathematical constraints derived from the frequency response functions. The optimization focuses on achieving fixed points where the response amplitudes are constrained to remain within specified bounds, thereby minimizing peak vibration levels. By explicitly considering harmonic excitations, this method ensures that the absorber is not only effective under specific loading conditions but also resilient against periodic and resonant forces. The resulting closed-form solutions enable precise parameter tuning, offering enhanced vibration suppression and energy harvesting capabilities across a wide range of excitation frequencies.

In the H_∞ optimization technique, the damping ratio of the primary structure is assumed to be zero ($\zeta = 0$) to simplify mathematical derivations and enable closed-form analytical solutions for the optimal tuning frequency and damping ratio of the damper. This assumption eliminates the influence of inherent structural damping, isolating the contribution of the damper in vibration control and ensuring precise optimization parameters. The controlled structure

is subjected to harmonic excitations, making the H_∞ optimization method particularly effective for minimizing the maximum dynamic response under these conditions (Den Hartog 1956). Eqs. (6) and (9) are rearranged to isolate and eliminate constraints, yielding simplified expressions for further analysis. These rearranged forms facilitate the derivation of critical parameters by decoupling the system's dynamic behavior from imposed limitations, enabling the precise determination of the optimal tuning frequency and damping ratio

$$|W_s| = \sqrt{\frac{a_0 + a_1\xi + a_2\xi^2}{b_0 + b_1\xi + b_2\xi^2}} \tag{15}$$

where the values of a_0 to b_2 are derived as follows, representing the coefficients of the rearranged equations that define the system's dynamic response. These coefficients incorporate key parameters such as the absorber's mass, stiffness, damping properties, and excitation frequency, providing the foundation for optimizing the absorber's performance through analytical techniques

$$\begin{aligned} a_0 &= \chi^4\delta^2\eta^2\kappa^4 + 2\chi^4\delta^2\eta^2\kappa^2 - 2\chi^2\delta^2\eta^4\kappa^2 + \chi^4\delta^2\eta^2 - 2\chi^2\delta^2\eta^4 + \delta^2\eta^6 + \chi^6 - 2\chi^4\eta^2 + \chi^2\eta^4, \\ a_1 &= 4\chi^4\delta\eta^2\kappa^2, \quad \text{and} \quad a_2 = (4\chi^2\delta^2\eta^4 + 4\chi^4\eta^2) \end{aligned} \tag{16}$$

$$\begin{aligned} b_0 = {} & \Upsilon^2\chi^8\delta^2\eta^2\kappa^4 - 2\Upsilon\chi^6\delta^2\eta^4\kappa^4 - 2\Upsilon^2\chi^6\delta^2\eta^4\kappa^2 + \chi^4\delta^2\eta^6\kappa^4 - 2\Upsilon\chi^6\delta^2\eta^4\kappa^2 + 2\Upsilon\chi^6\delta^2\eta^2\kappa^4 + 4\Upsilon\chi^4\delta^2\eta^6\kappa^2 + \Upsilon^2\chi^4\delta^2\eta^6 + 2\chi^4\delta^2\eta^6\kappa^2 \\ & - 2\chi^4\delta^2\eta^4\kappa^4 + \chi^2\eta^4 - 2\chi^2\delta^2\eta^8\kappa^2 + 2\Upsilon\chi^6\delta^2\eta^2\kappa^2 + 2\Upsilon\chi^4\delta^2\eta^6 - 4\Upsilon\chi^4\delta^2\eta^4\kappa^2 - 2\Upsilon\chi^2\delta^2\eta^8 + \Upsilon^2\chi^6\eta^4 + \chi^4\delta^2\eta^6 - 4\chi^4\delta^2\eta^4\kappa^2 \\ & + \chi^4\delta^2\eta^2\kappa^4 - 2\chi^2\delta^2\eta^8 + 4\chi^2\delta^2\eta^6\kappa^2 - 2\chi^4\eta^2 + \delta^2\eta^{10} + 2\Upsilon\chi^6\eta^4 - 2\Upsilon\chi^4\delta^2\eta^4 - 2\Upsilon\chi^4\eta^6 + 2\Upsilon\chi^2\delta^2\eta^6 + \chi^6\eta^4 - 2\chi^4\delta^2\eta^4 \\ & + 2\chi^4\delta^2\eta^2\kappa^2 - 2\chi^4\eta^6 + 4\chi^2\delta^2\eta^6 - 2\chi^2\delta^2\eta^4\kappa^2 + \chi^2\eta^8 - 2\delta^2\eta^8 - 2\Upsilon\chi^6\eta^2 + 2\Upsilon\chi^4\eta^4 - 2\chi^6\eta^2 + \chi^4\delta^2\eta^2 + 4\chi^4\eta^4 - 2\chi^2\delta^2\eta^4 \\ & - 2\chi^2\eta^6 + \delta^2\eta^6 + \chi^6 \end{aligned} \tag{17}$$

$$\begin{aligned} b_1 &= 4\chi^4\delta\eta^6\kappa^2 - 8\chi^4\eta^4\kappa^2\delta + 4\chi^4\delta\eta^2\kappa^2 \quad \text{and} \\ b_2 &= 4\Upsilon^2\chi^6\eta^4\kappa^4\delta^2 - 8\Upsilon^2\chi^4\eta^6\kappa^2\delta^2 - 8\Upsilon\chi^4\delta^2\eta^6\kappa^2 + 4\Upsilon^2\chi^2\delta^2\eta^8 + 8\Upsilon\chi^4\delta^2\eta^4\kappa^2 + 8\Upsilon\chi^2\delta^2\eta^8 + 4\Upsilon^2\chi^4\eta^6 + 4\chi^2\delta^2\eta^8 + 8\Upsilon\chi^4\eta^6 \\ & - 8\Upsilon\chi^2\delta^2\eta^6 + 4\chi^4\eta^6 - 8\chi^2\delta^2\eta^6 - 8\Upsilon\chi^4\eta^4 - 8\chi^4\eta^4 + 4\chi^2\delta^2\eta^4 + 4\chi^4\eta^2 \end{aligned} \tag{18}$$

The damping of the absorbers is set to $\xi = 0$ and $\xi = \infty$ to determine the fixed points, which represent the bounds of the system's dynamic response. These fixed-point conditions are then substituted into Eq. (15), allowing for a mathematical formulation that expresses the system's response under these extreme damping scenarios. The resulting expressions serve as critical benchmarks for evaluating and optimizing the absorber's performance

$$\lim_{\xi\to 0}|W_s| = \frac{a_0}{b_0} \quad \text{and} \quad \lim_{\xi\to\infty}|W_s| = \frac{a_2}{b_2} \tag{19}$$

Two mathematical constraints are derived from Eq. (19), which are expressed as follows. These constraints establish relationships between the system's parameters, including the absorber's mass ratio, frequency ratio, and damping characteristics. They serve as essential conditions for ensuring the optimal design and performance of the absorber under specified dynamic loading scenarios

$$\left(\frac{a_0}{b_0}\right)|_{\eta_{j,k}} = \left(\frac{a_2}{b_2}\right)|_{\eta_{j,k}} \quad \text{and} \quad \left(\frac{a_2}{b_2}\right)|_{\eta_j} = \left(\frac{a_2}{b_2}\right)|_{\eta_k} \tag{20}$$

where j, $k = 1, 2$. By applying the first constraint from Eq. (20), an analytical expression is derived. This expression captures the interdependence of key parameters, such as the absorber's frequency ratio and mass ratio, providing a foundation for optimizing the absorber's performance under specific dynamic conditions

$$\begin{aligned} & (\Upsilon^2\delta^2 + 2\Upsilon\delta^2 + \delta^2)\eta^6 + (-2\chi^2\delta^2\kappa^2\Upsilon^2 - 2\Upsilon\chi^2\delta^2\kappa^2 + \Upsilon^2\chi^2 + 2\Upsilon\chi^2 - 2\Upsilon\delta^2 + \chi^2 - 2\delta^2)\eta^4 \\ & + (\kappa^4\delta^2\chi^4\Upsilon^2 + 2\Upsilon\chi^2\delta^2\kappa^2 - 2\Upsilon\chi^2 - 2\chi^2 + \delta^2) + \eta^2\chi^2 = 0 \end{aligned} \tag{21}$$

Eq. (21) has been rewritten as follows to provide a simplified and more tractable form for further analysis. This reformulation highlights the relationships between the absorber's parameters, making it easier to interpret and apply the results to optimize the system's performance

$$\begin{aligned} & \eta^6 + (-\eta_1^2 - \eta_2^2 - \eta_3^2)\eta^4 + (\eta_1^2\eta_2^2 + \eta_1^2\eta_3^2 + \eta_2^2\eta_3^2)\eta^2 - \eta_1^2\eta_2^2\eta_3^2 = 0, \qquad \eta_1^2 + \eta_2^2 + \eta_3^2 = \frac{\chi^2(2\delta^2\kappa^2 - 1)\Upsilon - \chi^2 + 2\delta^2}{(\Upsilon + 1)\delta^2}, \\ & \eta_1^2\eta_2^2 + \eta_1^2\eta_3^2 + \eta_2^2\eta_3^2 = \frac{\chi^4\delta^2\kappa^4\Upsilon^2 + 2\chi^2(\delta^2\kappa^2 - 1)\Upsilon - 2\chi^2 + \delta^2}{\delta^2(\Upsilon + 1)^2}, \quad \text{and} \quad \eta_1^2\eta_2^2\eta_3^2 = -\frac{\chi^2}{\delta^2(\Upsilon + 1)^2} \end{aligned} \tag{22}$$

The second constraint of Eq. (20) is applied, leading to the derivation of an expression that further refines the relationships between the absorber's parameters. This expression plays a crucial role in ensuring that the absorber's design satisfies the necessary conditions for optimal performance under dynamic loading scenarios

$$\eta_1^2 + \eta_2^2 = 0 \tag{23}$$

Eq. (23) is substituted into Eq. (22), resulting in the derivation of the optimal frequency ratio of the absorber. This derived expression provides a critical parameter for tuning the absorber to achieve maximum vibration suppression and energy harvesting efficiency under dynamic loading conditions

$$\begin{aligned}&(2\Upsilon^4\delta^4\kappa^6 + 2\Upsilon^3\delta^4\kappa^6 - \Upsilon^4\delta^2\kappa^4 - 2\Upsilon^3\delta^2\kappa^4 - \Upsilon^2\delta^2\kappa^4)\chi^6 + (6\Upsilon^3\delta^4\kappa^4 + 6\Upsilon^2\delta^4\kappa^4 - 6\Upsilon^3\delta^2\kappa^2 - 12\Upsilon^2\delta^2\kappa^2 - 6\Upsilon\delta^2\kappa^2\\ &+ 2\Upsilon^3 + 6\Upsilon^2 + 6\Upsilon + 2)\chi^4 + (6\Upsilon^2\delta^4\kappa^2 + 6\Upsilon\delta^4\kappa^2 - 4\Upsilon^2\delta^2 - 8\Upsilon\delta^2 - 4\delta^2)\chi^2 + 2\Upsilon\delta^4 + 2\delta^4 = 0\end{aligned} \tag{24}$$

Eq. (24) has been rewritten to provide a more concise and interpretable form, facilitating the derivation of the absorber's optimal frequency ratio. This reformulation highlights the interdependence of the system parameters and serves as a key step in optimizing the absorber's dynamic performance

$$\begin{aligned}&A(\chi^2)^3 + B(\chi^2)^2 + C\chi^2 + E = 0\\ &(\chi)_{\text{opt}} = \sqrt{\frac{(-108EA^2 + 36CBA + 12\sqrt{3}A_1A - 8B^3)^{\frac{1}{3}}}{6A} - \frac{2(3AC - B^2)}{3A(-108EA^2 + 36CBA + 12\sqrt{3}A_1A - 8B^3)^{\frac{1}{3}}} - \frac{B}{3A}}\\ &A_1 = \sqrt{27A^2E^2 - 18ABCE + 4AC^3 + 4B^3E - B^2C^2}\end{aligned} \tag{25}$$

By applying Eqs. (22) and (23), the closed-form expressions for η_1^2, η_2^2, and η_3^2 are derived. These expressions provide explicit relationships between the absorber's design parameters and the dynamic characteristics of the system, offering a foundational basis for optimizing the absorber's performance across various operational scenarios

$$\begin{aligned}\eta_{1,2}^2 &= \pm\sqrt{\frac{\chi^2}{2(\Upsilon+1)((\Upsilon\kappa^2\delta^2 - \frac{1}{2}\Upsilon - \frac{1}{2})\chi^2 + \delta^2)}}\\ \eta_3^2 &= \frac{\chi^2(2\delta^2\kappa^2 - 1)\Upsilon - \chi^2 + 2\delta^2}{(\Upsilon+1)\delta^2}\end{aligned} \tag{26}$$

Eq. (26) is utilized to derive the optimal damping ratio of the absorber in the form of a closed-form expression. To achieve this, the square of the resultant from Eq. (15) is differentiated with respect to the roots of the equation, as defined by Eq. (26). This process ensures an accurate determination of the damping ratio, which is critical for optimizing the absorber's vibration suppression efficiency

$$\frac{\partial|W_s|^2}{\partial\eta^2}|_{\eta_{1,2,3}^2} = 0 \quad \text{and} \quad (\xi)_{\text{opt}}\sqrt{\frac{\xi_1^2 + \xi_2^2 + \xi_3^2}{3}} \tag{27}$$

By applying the first expression of Eq. (27), the closed-form expression for the damping ratio of the absorber is derived. This expression provides a precise mathematical formulation for determining the optimal damping ratio of the absorber

$$\begin{aligned}\xi_{1,2,3}^2 = \frac{\begin{array}{c}(3\Upsilon^2\chi^2\delta^3\kappa^2 + 6\Upsilon\chi^2\delta^3\kappa^2 + 4\chi^2\delta^3\kappa^2)\eta_{1,2,3}^4\\ +(-4\Upsilon^2\chi^4\delta^3\kappa^4 - 4\Upsilon\chi^4\delta^3\kappa^4 + 2\Upsilon^2\chi^4\delta\kappa^2 + 4\Upsilon\chi^4\delta\kappa^2 - 4\Upsilon\chi^2\delta^3\kappa^2 + 4\chi^4\delta\kappa^2 - 4\chi^2\delta^3\kappa^2)\eta_{1,2,3}^2\\ +\Upsilon^2\chi^6\delta^3\kappa^6 + 2\Upsilon\chi^4\delta^3\kappa^4 - 2\Upsilon\chi^4\delta\kappa^2 - 4\chi^4\delta\kappa^2\end{array}}{\begin{array}{c}(8\Upsilon^2\delta^4 + 16\Upsilon\delta^4 + 8\delta^4)\eta_{1,2,3}^6\\ +(-8\Upsilon^2\chi^2\delta^4\kappa^2 - 8\Upsilon\chi^2\delta^4\kappa^2 + 16\Upsilon^2\chi^2\delta^2 + 32\Upsilon\chi^2\delta^2 - 8\Upsilon\delta^4 + 16\chi^2\delta^2 - 8\delta^4)\eta_{1,2,3}^4\\ +(-16\Upsilon^2\chi^4\delta^2\kappa^2 - 16\Upsilon\chi^4\delta^2\kappa^2 + 8\Upsilon^2\chi^4 + 16\Upsilon\chi^4 - 16\Upsilon\chi^2\delta^2 + 8\chi^4 - 16\chi^2\delta^2)\eta_{1,2,3}^2\\ +4\Upsilon^2\chi^6\delta^2\kappa^4 + 8\Upsilon\chi^4\delta^2\kappa^2 - 8\Upsilon\chi^4 - 8\chi^4\end{array}}\end{aligned} \tag{28}$$

The optimization of frequency and damping ratios for inertially amplified absorbers plays a crucial role in achieving effective vibration suppression and energy harvesting. This section integrates insights from the analyses of both H_2 and H_∞ optimization methods, focusing on the interplay between absorber mass ratios and inertial angles to provide practical design recommendations.

Frequency Ratios

Figs. 2(a) and 3(a) depict the variations in H_2 and H_∞ optimized frequency ratios, respectively, as functions of absorber mass ratios for various inertial angles. A consistent trend can be observed: as the absorber mass ratio increased, the optimal frequency ratio decreased. This behavior is attributed to the enhanced inertial effect of the absorber, which lowers the resonance frequency of the coupled system, thereby improving vibration mitigation capabilities. Conversely, an increase in the inertial angle raised the optimal frequency ratio due to the geometric stiffness contribution introduced by larger inertial angles. This stiffness counteracts the mass-induced frequency reduction, shifting the optimal frequency upward.

The opposing trends underscore the coupled influence of inertial angles and mass ratios on the absorber's dynamic response. To achieve desired performance, a balance must be struck between increasing mass ratios, which favor lower frequencies for better mitigation, and inertial angles, which introduce stiffness contributions to manage system stability. For practical applications, moderately high mass ratios combined with small to moderate inertial angles

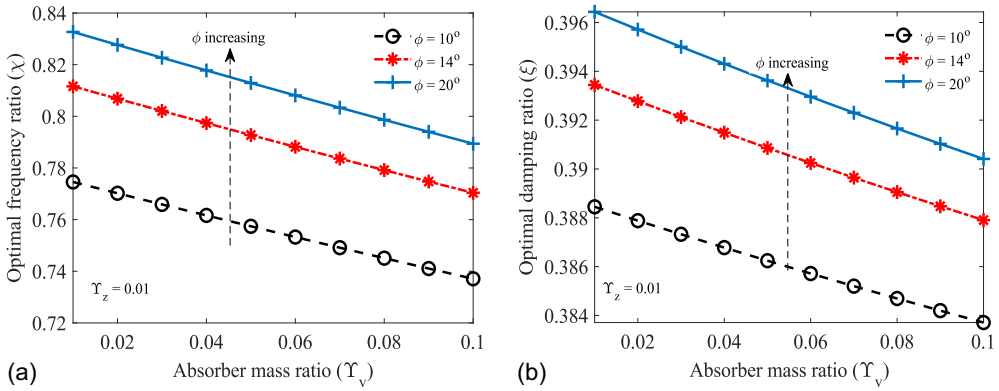

Fig. 2. H_2 optimized (a) frequency; and (b) damping ratios derived by varying the absorber mass ratio. The inertial angles were changed from 10° to 14°, and 20° to determine the changes in the optimal frequency ratios.

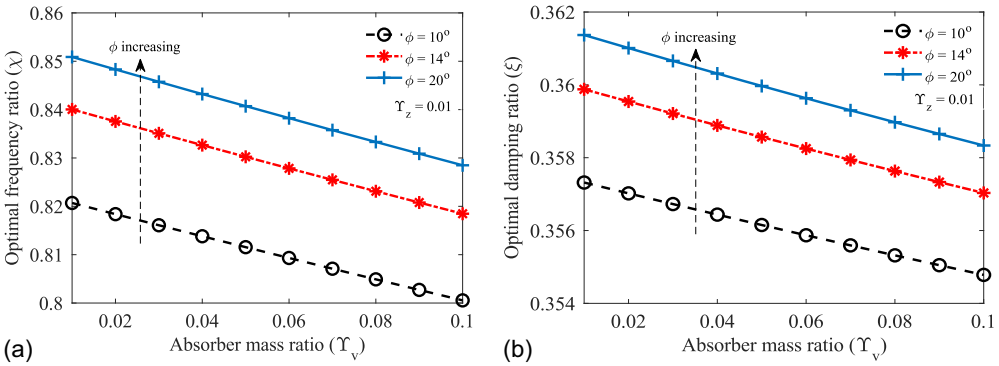

Fig. 3. Optimal (a) frequency; and (b) damping ratios are determined by adjusting the absorber mass ratio, and the inertial angles were varied at 10°, 14°, and 20° to observe their effect on the optimal frequency ratios. H_∞ optimized design parameters are considered for this study.

are recommended to balance these effects and ensure optimal tuning.

Damping Ratios

Figs. 2(b) and 3(b) illustrate the variations in H_2 and H_∞ optimized damping ratios against absorber mass ratios for different inertial angles. A clear trend emerged: as the absorber mass ratio increased, the optimal damping ratio decreased. This reduction is due to the dominance of the absorber's mass in energy transfer dynamics, requiring less damping to achieve effective vibration suppression. In contrast, an increase in the inertial angle led to higher optimal damping ratios. Larger inertial angles amplify dynamic coupling effects and increase energy dissipation demands within the absorber. The dependency of damping ratios on both mass ratio and inertial angle highlights the need for carefully designed damping mechanisms that complement the absorber's mass and inertial effects. Practical recommendations include designing systems with moderate damping ratios for high mass ratios and slightly higher damping ratios for configurations with significant inertial angles. This balance ensures effective energy dissipation without overdamping the system.

Comparative Insights

The comparative analysis between H_2 and H_∞ optimization revealed that although both methods exhibited similar trends in frequency and damping variations, their applicability depends on the excitation conditions. The H_2 method focuses on minimizing system response variance under stochastic excitations, making it suitable for applications involving random, nonharmonic forces. On the other hand, the H_∞ method targets minimizing maximum dynamic response under harmonic excitations, favoring scenarios dominated by periodic or resonant forces.

Practical Recommendations

Based on the observed trends and performance characteristics, the following recommendations can be made:

- Energy harvesting capacity: To maximize energy harvesting, systems should integrate piezoelectric stacks with high coupling coefficients and moderate inertial angles to enhance both mechanical-to-electrical energy conversion and dynamic response stability.
- Frequency ratios: For applications requiring broad vibration mitigation, a higher absorber mass ratio (e.g., 0.06–0.1) with a small to moderate inertial angle (e.g., 5°–20°) is recommended.
- Damping ratios: Systems with higher absorber mass ratios should employ lower damping values, whereas those with significant inertial angles should integrate mechanisms for enhanced energy dissipation.
- Optimization approach: Use H_2 optimization for stochastic environments and H_∞ optimization for harmonic excitations.

These recommendations aim to balance frequency tuning, damping effectiveness, and structural constraints, ensuring the absorber's optimal performance across diverse engineering applications.

Table 1. Optimal design parameters of the absorbers from H_2 optimization

Absorber name	References	χ	ξ
IAEHDVA	This study	0.7616	0.3867
TMD	Iwata (1982) and Warburton (1982)	0.9574	0.1198
TMD	Warburton (1982) and Zilletti et al. (2012)	0.9713	0.1225

Table 2. H_∞ optimized system parameters for the novel absorbers

Absorber name	References	χ	ξ
IAEHDVA	This study	0.8138	0.3564
TMD	Ormondroyd and Den Hartog (1928) and Nishihara and Asami (2002)	0.9434	0.1457
TMD	Krenk (2005)	0.9434	0.1682

Table 3. Design parameters for the piezoelectric stack

Parameter	Value	Unit
δ	0.8649	—
β	-4.57×10^{-3}	NV^{-1}
τ	4.3×10^{-8}	F
R_v	3×10^4	Ω
κ^2	0.33	—

Evaluation of Dynamic Responses

The optimum IAEHDVAs were installed at the top of the SDOF system to control their dynamic responses. The structural system parameters of the SDOF systems were considered the same and the damping ratio of the SDOF system was considered as 0.01, i.e., $\zeta = 0.01$. The vibration reduction capacity of the novel damper is compared with the dynamic response reduction capacity of the conventional damper. To make a fair comparison, the total mass ratio of each damper was considered the same, i.e., $\Upsilon_v + 2\Upsilon_z = \Upsilon_D = 0.06$. Further, these values were substituted in the exact closed-form expressions of the damper's optimal frequency and damping ratios.

The H_2 optimized conventional TMDs were developed by Iwata (1982), Warburton (1982), and Zilletti et al. (2012). The H_∞ optimized TMD were developed by Ormondroyd and Den Hartog (1928), Nishihara and Asami (2002), and Krenk (2005). The H_2 and H_∞ optimized design parameters of the novel dampers are derived in this study. The H_2 and H_∞ optimized design parameters of all dampers are listed in Tables 1 and 2. The design parameters for the piezoelectric stack (Ali and Adhikari 2013; Adhikari et al. 2009) and the harvester (Ali et al. 2010) are listed in Table 3.

The optimal structural displacements of the SDOF systems controlled by the H_2 and H_∞ dampers are presented in Figs. 4(a and b), respectively. These results were derived under harmonic excitation, which imposes periodic forces on the system. The analysis demonstrates how the dampers effectively mitigate vibrations by tuning the system's response to the excitation frequency, thereby reducing structural displacements. The comparative performance of the H_2 and H_∞ dampers under these conditions underscores their suitability for vibration control in scenarios dominated by harmonic forces. According to Fig. 4(a), the maximum displacement of the uncontrolled SDOF system was derived as 50. The maximum displacements of the SDOF systems controlled by the H_2 optimized TMDs and IAEHDVA have been derived as 7.62, 7.07, and 4.87. Hence, after comparing these maximum values, it has been found that the IAEHDVA is 36.09% and 31.11% superior to the TMDs.

According to the Fig. 4(b), the maximum displacement of the uncontrolled SDOF system was derived as 50. The maximum displacements of the SDOF systems controlled by the H_∞ optimized TMDs and IAEHDVA have been derived as 6.22, 6.20, and 4.56. Hence, after comparing these maximum values, it has been found that the IAEHDVA is 26.69% and 26.45% superior to the TMDs.

The Clough–Penzien power spectrum, a modified version of the widely used Kanai–Tajimi spectrum, was employed as the ground acceleration for the evaluation of the IAEHDVA's performance. This spectrum introduces a secondary filtering mechanism that enhances the representation of ground motion by incorporating a unilateral power spectral density (PSD), which accounts for nonreciprocal energy distribution in the frequency domain

$$P_{\ddot{x}_g} = S_0 \frac{\omega_p^4 + 4\zeta_p^2\omega_p^2\omega^2}{(\omega_p^2 - \omega^2)^2 + 4\zeta_p^2\omega_p^2\omega^2} \frac{\omega^4}{(\omega_v^2 - \omega^2)^2 + 4\zeta_v^2\omega_v^2\omega^2} \tag{29}$$

The constant power spectral density for random white noise excitation is denoted by S_0 $[(\mathrm{m/s^2})^2/\mathrm{Hz}]$. The parameters of the widely recognized Kanai–Tajimi model, ω_p [natural frequency (rad/s)] and ζ_p (damping ratio, dimensionless), represent the dynamic characteristics of the soil layer. A secondary filter, characterized by ω_v and ζ_v, modifies the power spectral density to produce a constrained power output for ground displacement. Given that

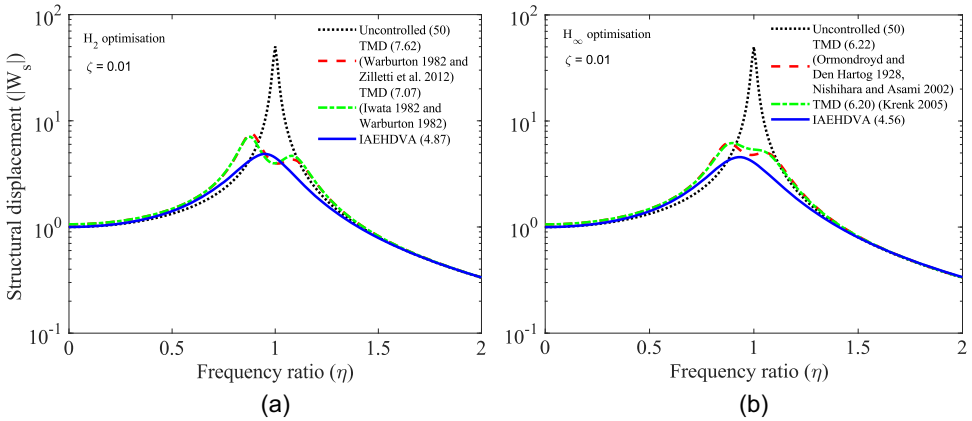

Fig. 4. Optimal structural displacements of the SDOF systems controlled by the (a) H_2; and (b) H_∞ optimized dampers.

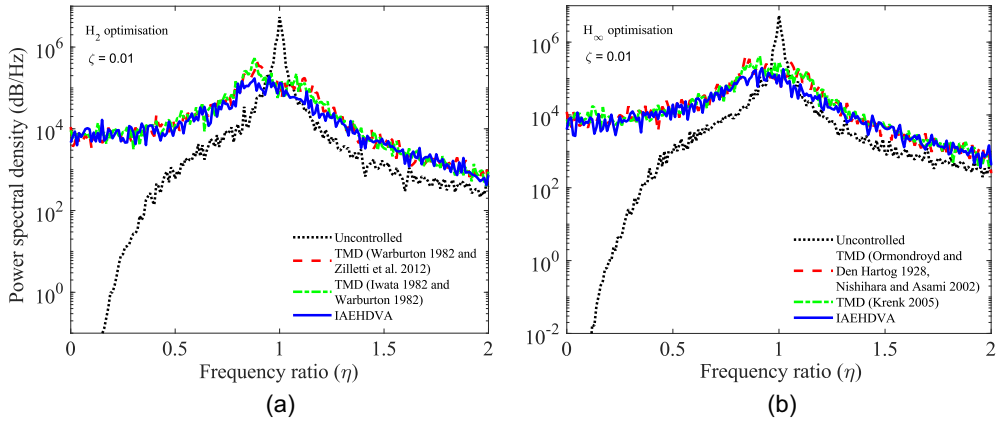

Fig. 5. Optimal structural displacements of the SDOF systems controlled by the (a) H_2; and (b) H_∞ optimized dampers subjected to random excitation.

$\omega_v \ll \omega_p$, where ω_p is the primary soil frequency (rad/s), the second quotient rapidly approaches unity. Consequently, the influence of the secondary filter is predominantly confined to the very-low-frequency range of the spectrum.

The values of these filter parameters were sourced from Kiureghian and Neuenhofer (1992) to enable site-specific analyses for soils categorized as hard, medium, or soft. In this study, the focus is on soft soil. Accordingly, the optimal structural displacements of the SDOF systems controlled by the H_2 and H_∞ dampers subjected to random white noise are shown in Figs. 5(a and b). According to the Fig. 5(a), the maximum displacement of the uncontrolled SDOF system was derived as 5.429×10^6 dB/Hz. The maximum displacements of the SDOF systems controlled by the H_2 optimized TMDs and IAEHDVA have been derived as 4.567×10^5, 5.342×10^5, and 1.91×10^5 dB/Hz. Hence, after comparing these maximum values, it has been found that the IAEHDVA is 58.16% and 64.23% superior to the TMDs.

According to Fig. 5(b), the maximum displacements of the SDOF systems controlled by the H_∞ optimized TMDs and IAEHDVA have been derived as 3.742×10^5, 4.137×10^5, and 1.951×10^5 dB/Hz. Hence, after comparing these maximum values, it has been found that the IAEHDVA is 47.85% and 52.83% superior to the TMDs.

The vibration reduction capacity of the optimum IAEHDVA is further analyzed with the well-established conventional EHDVA (Ali and Adhikari 2013) and inerter-based energy harvesting dynamic vibration absorbers (IEHDVA) (Giaralis 2021). The optimal system parameters are listed in Table 4.

Table 4. Optimal design parameters of the novel and conventional absorbers

Absorber name	χ	ξ
IAEHDVA[a]	0.7616	0.3867
EHDVA	0.9434	0.0956
IEHDVA	0.9642	0.1071

[a]This study.

The optimal structural displacements of the SDOF systems controlled by the IEHDVA, EHDVA, and IAEHDVA subjected to harmonic and random excitations are shown in Figs. 6(a and b). According to Fig. 6(a), the maximum displacements of the SDOF systems controlled by the IEHDVA, EHDVA, and IAEHDVA have been derived as 20.42, 7.89, and 4.87. Hence, after comparing these maximum values, it has been found that the IAEHDVA is 76.15% and 38.30% superior to the IEHDVA and EHDVA. According to Fig. 6(b), the maximum displacements of the SDOF systems controlled by the IEHDVA, EHDVA, and IAEHDVA have been derived as 5.53×10^5, 1.076×10^5, and 3.81×10^4. Hence, after comparing these maximum values, it has been found that the IAEHDVA is 93.10% and 64.56% superior to the IEHDVA and EHDVA.

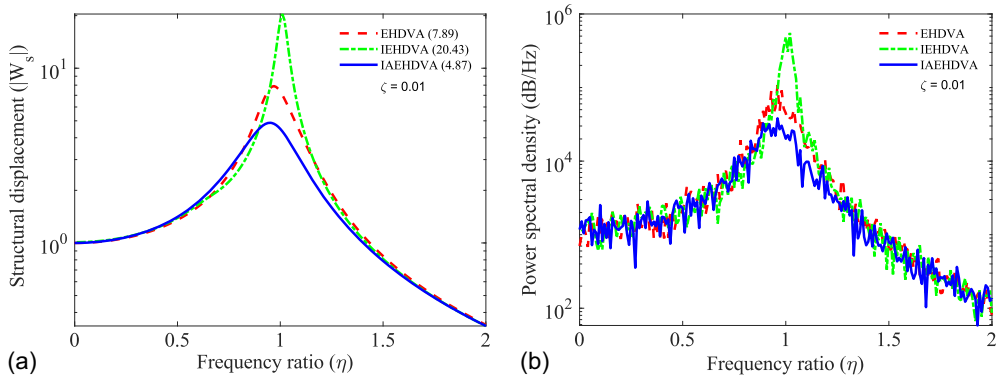

Fig. 6. Optimal structural displacements of the SDOF systems controlled by the IEHDVA, EHDVA, and IAEHDVA subjected to (a) harmonic; and (b) random excitations.

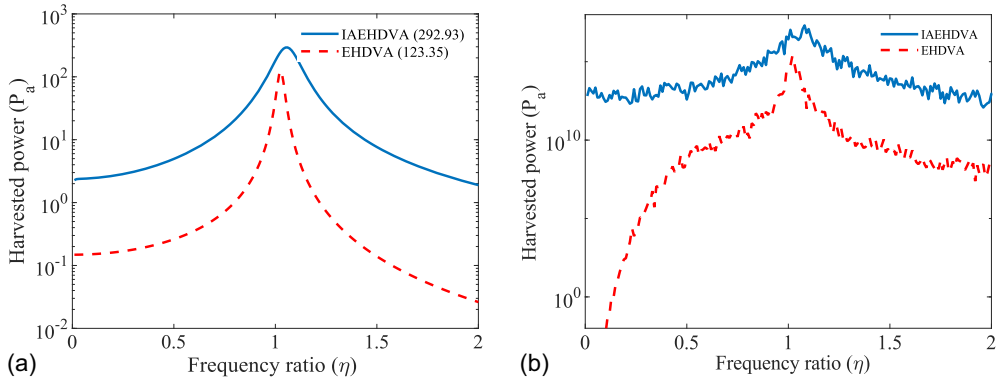

Fig. 7. Optimal harvested power of the absorbers versus frequency ratio: (a) harmonic; and (b) random excitation applied to the controlled structures.

Harvested Power

The harvested power using IAEHDVA has been derived as follows:

$$P_a = \frac{|V|^2}{R_v} = \frac{|V|^2}{\delta}\tau\nu \tag{30}$$

The optimal harvested power of the absorbers versus frequency ratio is shown in Fig. 7. Eqs. (8) and (30) were applied to achieve these graphs. According to Fig. 7(a), the maximum harvested power using IAEHDVA and EHDVA achieved was 292.93 and 123.35. Hence, IAEHDVA has a 57.89% higher energy harvesting capacity than EHDVA subjected to harmonic excitation. According to Fig. 7(b), the maximum harvested power using IAEHDVA and EHDVA achieved was 2.06×10^{17} and 2.367×10^{15} dB/Hz. Hence, IAEHDVA has a 98.85% higher energy harvesting capacity than EHDVA subjected to random excitation.

Summary and Conclusions

This study introduced the IAEHDVA, a novel device that integrates vibration mitigation with energy harvesting capabilities. Using inertial amplifiers, the IAEHDVA achieves effective mass amplification without increasing the physical size of the absorber, addressing key limitations of conventional and inerter-based TMD systems. The incorporation of piezoelectric stacks enhances its functionality by converting mechanical vibrations into electrical energy, contributing to the development of sustainable and self-sufficient systems. Advanced H_2 and H_∞ optimization methods were employed to derive closed-form solutions for optimal tuning and damping ratios, ensuring precise performance under both harmonic and stochastic excitations. Comparative analyses demonstrated that the IAEHDVA outperformed traditional vibration absorbers, achieving up to 64.23% greater vibration suppression and 98.85% higher energy harvesting efficiency.

The practical applicability of the IAEHDVA spans multiple engineering domains, including structural resilience in seismic and wind-prone environments, as well as renewable energy systems like offshore wind turbines. By addressing challenges related to space, weight, and energy efficiency, the IAEHDVA aligns with global sustainability objectives and the transition toward Net-Zero infrastructure. Future work will focus on exploring the nonlinear dynamics of the IAEHDVA and extending its application to more complex systems, such as multiple-degree-of-freedom structures and hybrid renewable energy platforms.

Appendix. Closed-Form Expressions from Eqs. (10) and (14)

$$\begin{aligned}
S_1 = {} & 8\xi^3\delta^2\chi^6\Upsilon^3\kappa^2 + 4\delta^3\xi^2\chi^6\kappa^4\Upsilon + 16\xi^3\delta^2\chi^6\kappa^2\Upsilon^2 + 8\xi^3\delta^4\chi^4\kappa^2\Upsilon^2 + 4\delta^3\chi^4\xi^2\kappa^4\Upsilon^2 + 2\xi\delta^4\chi^4\kappa^6 + 2\xi\delta^2\kappa^4\chi^6\Upsilon + 8\xi^3\delta^2\chi^6\kappa^2\Upsilon \\
& + 8\xi^3\delta^4\chi^4\kappa^2\Upsilon + 8\delta^3\chi^4\xi^2\kappa^4\Upsilon - 4\xi\delta^2\chi^6\kappa^2\Upsilon^2 + 4\delta\chi^6\kappa^2\Upsilon^2\xi^2 + 16\delta^3\chi^4\kappa^2\Upsilon^2\xi^2 + 16\xi^3\delta^2\chi^4\kappa^2\Upsilon^2 + 6\xi\delta^4\chi^4\kappa^4 + \delta^3\chi^4\kappa^6 \\
& + 12\delta^3\chi^4\xi^2\kappa^4 + 2\xi\delta^2\chi^6\Upsilon^3 + 4\delta\chi^6\Upsilon^3\xi^2 - 2\xi\delta^2\chi^6\kappa^2\Upsilon + 4\delta\chi^6\kappa^2\Upsilon\xi^2 + 4\xi\delta^4\chi^4\kappa^2\Upsilon - 2\delta^3\chi^4\kappa^4\Upsilon + 28\delta^3\chi^4\kappa^2\Upsilon\xi^2 + 2\xi\delta^2\chi^4\kappa^4\Upsilon \\
& + 32\xi^3\delta^2\chi^4\kappa^2\Upsilon + 8\xi^3\delta^4\chi^2\kappa^2\Upsilon + 6\xi\delta^2\chi^6\Upsilon^2 + 12\delta\chi^6\xi^2\Upsilon^2 + 2\xi\delta^4\chi^4\Upsilon^2 + \delta^3\chi^4\kappa^2\Upsilon^2 + 4\delta^3\chi^4\xi^2\Upsilon^2 + 2\xi\delta^2\chi^4\kappa^2\Upsilon^2 + 8\xi^3\delta^2\chi^4\Upsilon^2 \\
& + 16\delta\chi^4\Upsilon^2\xi^4 + 2\xi\delta^2\kappa^2\chi^6 + 6\xi\delta^4\kappa^2\chi^4 + 2\delta^3\chi^4\kappa^4 + 16\delta^3\kappa^2\xi^2\chi^4 + 6\xi\delta^2\chi^4\kappa^4 + 24\xi^3\delta^2\kappa^2\chi^4 - 4\xi\delta^4\chi^2\kappa^4 + 8\xi^3\delta^4\chi^2\kappa^2 + 6\xi\delta^2\chi^6\Upsilon \\
& + 12\delta\chi^6\Upsilon\xi^2 + 4\xi\delta^4\chi^4\Upsilon - \delta^3\chi^4\kappa^2\Upsilon + 8\delta^3\chi^4\Upsilon\xi^2 + 2\xi\delta^2\chi^4\kappa^2\Upsilon + 16\xi^3\delta^2\chi^4\Upsilon + 8\delta\chi^4\kappa^2\Upsilon\xi^2 + 32\delta\chi^4\xi^4\Upsilon + 8\xi^3\delta^4\chi^2\Upsilon \\
& + 4\delta^3\chi^2\kappa^2\Upsilon\xi^2 + 16\delta^3\chi^2\xi^4\Upsilon + 2\xi\chi^6\Upsilon^2 - 4\delta\chi^4\xi^2\Upsilon^2 + 2\xi\delta^2\chi^6 + \delta\chi^6\kappa^2 + 4\delta\chi^6\xi^2 + 2\xi\delta^4\chi^4 + \delta^3\kappa^2\chi^4 + 4\delta^3\chi^4\xi^2 + 8\xi^3\delta^2\chi^4 \\
& + 12\delta\chi^4\kappa^2\xi^2 + 16\delta\chi^4\xi^4 - 8\xi\delta^4\kappa^2\chi^2 + 8\xi^3\delta^4\chi^2 - 2\delta^3\chi^2\kappa^4 + 4\xi\chi^6\Upsilon - 4\delta^3\chi^2\kappa^2\xi^2 + 16\delta^3\chi^2\xi^4 - 2\xi\delta^2\chi^4\Upsilon + \delta\chi^4\Upsilon\kappa^2 - 12\delta\chi^4\Upsilon\xi^2 \\
& + 8\xi^3\chi^4\Upsilon - 2\xi\delta^4\chi^2\Upsilon + 2\delta^3\Upsilon\chi^2\kappa^2 - 4\delta^3\chi^2\Upsilon\xi^2 + 2\xi\delta^2\Upsilon\chi^2\kappa^2 + 8\xi^3\delta^2\chi^2\Upsilon + 2\xi\chi^6 - 2\xi\delta^2\chi^4 - 2\delta\chi^4\kappa^2 - 8\delta\chi^4\xi^2 \\
& + 8\xi^3\chi^4 - 4\xi\delta^4\chi^2 - 2\delta^3\kappa^2\chi^2 - 8\delta^3\chi^2\xi^2 - 2\xi\delta^2\kappa^2\chi^2 + 8\xi^3\delta^2\chi^2 + 2\xi\delta^4\kappa^2 - 2\xi\chi^4\Upsilon + 4\delta\chi^2\Upsilon\xi^2 - 4\xi\chi^4 - 2\xi\delta^2\chi^2 + \delta\chi^2\kappa^2 + 4\delta\chi^2\xi^2 \\
& + 2\xi\delta^4 + \delta^3\kappa^2 + 4\delta^3\xi^2 + 2\xi\chi^2 + 2\xi\delta^2
\end{aligned} \tag{31}$$

$$
\begin{aligned}
S_2 = {} & 8\xi^3\delta^3\kappa^4\chi^6\Upsilon^3 + 4\Upsilon\chi^6\delta^4\kappa^6\xi^2 + 16\xi^3\delta^3\kappa^4\chi^6\Upsilon^2 + 2\xi\delta^3\kappa^6\chi^6\Upsilon + 8\xi^3\delta^3\chi^6\kappa^4\Upsilon - 4\xi\delta^3\kappa^4\chi^6\Upsilon^2 \\
& + 4\delta^2\kappa^4\chi^6\Upsilon^2\xi^2 + 8\xi^3\delta^3\kappa^4\chi^4\Upsilon^2 + 4\chi^4\delta^4\kappa^6\xi^2 + 2\xi\delta^3\kappa^2\chi^6\Upsilon^3 - 2\xi\delta^3\kappa^4\chi^6\Upsilon + 4\delta^2\xi^2\chi^6\kappa^4\Upsilon \\
& - 8\Upsilon\chi^4\delta^4\kappa^4\xi^2 + 16\xi^3\delta^3\kappa^4\chi^4\Upsilon + 6\xi\delta^3\kappa^2\chi^6\Upsilon^2 + 4\delta^2\kappa^2\chi^6\Upsilon^3\xi^2 + 12\delta^2\kappa^2\chi^6\Upsilon^2\xi^2 \\
& + 8\xi^3\delta^3\kappa^2\chi^4\Upsilon^2 + 16\delta^2\kappa^2\chi^4\xi^4\Upsilon^2 + 2\xi\delta^3\kappa^4\chi^6 + 8\xi^3\delta^3 + 4\chi^4\delta^4\kappa^4\xi^2 + 2\xi\delta^3\kappa^6\chi^4 \\
& + 16\xi^3\delta^3\kappa^4\chi^4 + 6\xi\delta^3\kappa^2\chi^6\Upsilon + 12\delta^2\kappa^2\chi^6\Upsilon\xi^2 - 8\xi\delta^3\kappa^4\chi^4\Upsilon + 16\xi^3\delta^3\kappa^2\chi^4\Upsilon \\
& + 4\delta^2\kappa^4\chi^4\Upsilon\xi^2 + 32\delta^2\kappa^2\chi^4\xi^4\Upsilon + 2\xi\chi^6\delta\kappa^2\Upsilon^2 + 6\xi\delta^3\kappa^2\chi^4\Upsilon^2 + 8\delta^2\kappa^2\chi^4\Upsilon^2\xi^2 \\
& + 2\xi\delta^3\kappa^2\chi^6 + \delta^2\kappa^4\chi^6 + 4\delta^2\kappa^2\chi^6\xi^2 + 8\xi^3\delta^3\kappa^2\chi^4 + 8\delta^2\kappa^4\chi^4\xi^2 + 16\delta^2\kappa^2\chi^4\xi^4 \\
& - 8\chi^2\delta^4\kappa^4\xi^2 + 4\xi\chi^6\delta\kappa^2\Upsilon + 6\xi\delta^3\kappa^2\chi^4\Upsilon - 4\xi\delta^3\kappa^4\chi^2 + 8\delta^2\kappa^2\chi^4\Upsilon\xi^2 + 8\xi^3\chi^4\delta\Upsilon\kappa^2 \\
& + 4\Upsilon\chi^2\delta^4\kappa^2\xi^2 + 2\xi\chi^6\delta\kappa^2 + 8\xi^3\chi^4\delta\kappa^2 - 8\chi^2\delta^4\kappa^2\xi^2 - 16\xi^3\delta^3\kappa^2\chi^2 + 4\xi\chi^4\delta\Upsilon\kappa^2 \\
& + 6\xi\delta^3\Upsilon\chi^2\kappa^2 + 4\delta^2\Upsilon\chi^2\kappa^2\xi^2 - 4\delta^2\kappa^2\chi^2\xi^2 + 4\delta^4\kappa^2\xi^2 + 4\delta^2\Upsilon\chi^2\xi^2 \\
& + 8\xi^3\chi^2\delta\Upsilon + 4\delta^2\chi^2\xi^2 + 2\xi\chi^2\delta\kappa^2 + 8\xi^3\chi^2\delta + 4\xi^2\delta^4 + 2\xi\delta^3\kappa^2 \\
& + 4\chi^2\xi^2 + 4\delta^2\xi^2
\end{aligned} \tag{32}
$$

$$
\begin{aligned}
S_4 = {} & -9\Upsilon^{12}\delta^{10}\kappa^{16} + 27\Upsilon^{10}\delta^{12}\kappa^{16} - 27\Upsilon^8\delta^{14}\kappa^{16} + 9\Upsilon^6\delta^{16}\kappa^{16} - 99\Upsilon^{11}\delta^{10}\kappa^{16} + 216\Upsilon^9\delta^{12}\kappa^{16} \\
& - 135\Upsilon^7\delta^{14}\kappa^{16} + 18\Upsilon^5\delta^{16}\kappa^{16} - 108\Upsilon^{12}\delta^{10}\kappa^{14} + 14\Upsilon^{12}\delta^8\kappa^{16} + 216\Upsilon^{10}\delta^{12}\kappa^{14} - 515\Upsilon^{10}\delta^{10}\kappa^{16} \\
& - 108\Upsilon^8\delta^{14}\kappa^{14} + 750\Upsilon^8\delta^{12}\kappa^{16} - 254\Upsilon^6\delta^{14}\kappa^{16} + 5\Upsilon^4\delta^{16}\kappa^{16} - 1{,}224\Upsilon^{11}\delta^{10}\kappa^{14} + 168\Upsilon^{11}\delta^8\kappa^{16} \\
& + 1{,}800\Upsilon^9\delta^{12}\kappa^{14} - 576\Upsilon^7\delta^{14}\kappa^{14} + 1{,}476\Upsilon^7\delta^{12}\kappa^{16} - 222\Upsilon^5\delta^{14}\kappa^{16} - 432\Upsilon^{12}\delta^{10}\kappa^{12} \\
& + 146\Upsilon^{12}\delta^8\kappa^{14} + 432\Upsilon^{10}\delta^{12}\kappa^{12} - 6{,}315\Upsilon^{10}\delta^{10}\kappa^{14} + 899\Upsilon^{10}\delta^8\kappa^{16} + 6{,}288\Upsilon^8\delta^{12}\kappa^{14} \\
& - 3{,}714\Upsilon^8\delta^{10}\kappa^{16} - 1{,}091\Upsilon^6\delta^{14}\kappa^{14} + 1{,}869\Upsilon^6\delta^{12}\kappa^{16} - 107\Upsilon^4\delta^{14}\kappa^{16} - 5{,}040\Upsilon^{11}\delta^{10}\kappa^{12} \\
& + 1{,}752\Upsilon^{11}\delta^8\kappa^{14} + 3{,}744\Upsilon^9\delta^{12}\kappa^{12} - 1{,}9575\Upsilon^9\delta^{10}\kappa^{14} + 2{,}830\Upsilon^9\delta^8\kappa^{16} + 1{,}2024\Upsilon^7\delta^{12}\kappa^{14} \\
& - 6{,}006\Upsilon^7\delta^{10}\kappa^{16} - 897\Upsilon^5\delta^{14}\kappa^{14} + 1{,}668\Upsilon^5\delta^{12}\kappa^{16} - 31\Upsilon^3\delta^{14}\kappa^{16} - 576\Upsilon^{12}\delta^{10}\kappa^{10} + 660\Upsilon^{12}\delta^8\kappa^{12} \\
& - 1{,}665\Upsilon^9\delta^{10}\kappa^{16} - 26{,}304\Upsilon^{10}\delta^{10}\kappa^{12} + 9{,}541\Upsilon^{10}\delta^8\kappa^{14} + 13{,}404\Upsilon^8\delta^{12}\kappa^{12} - 40{,}857\Upsilon^8\delta^{10}\kappa^{14} \\
& + 5{,}790\Upsilon^8\delta^8\kappa^{16} + 13{,}932\Upsilon^6\delta^{12}\kappa^{14} - 7{,}296\Upsilon^6\delta^{10}\kappa^{16} - 301\Upsilon^4\delta^{14}\kappa^{14} + 1{,}128\Upsilon^4\delta^{12}\kappa^{16} \\
& - 6{,}912\Upsilon^{11}\delta^{10}\kappa^{10} + 7{,}506\Upsilon^{11}\delta^8\kappa^{12} - 25\Upsilon^{11}\delta^6\kappa^{14} - 80{,}478\Upsilon^9\delta^{10}\kappa^{12} + 31{,}083\Upsilon^9\delta^8\kappa^{14} \\
& + 25{,}668\Upsilon^7\delta^{12}\kappa^{12} - 61{,}029\Upsilon^7\delta^{10}\kappa^{14} + 7{,}968\Upsilon^7\delta^8\kappa^{16} + 10{,}306\Upsilon^5\delta^{12}\kappa^{14} - 6{,}900\Upsilon^5\delta^{10}\kappa^{16} \\
& - 27\Upsilon^3\delta^{14}\kappa^{14} + 552\Upsilon^3\delta^{12}\kappa^{16} + 1{,}775\Upsilon^{12}\delta^8\kappa^{10} - 171\Upsilon^{12}\delta^6\kappa^{12} - 37{,}055\Upsilon^{10}\delta^{10}\kappa^{10} \\
& + 39{,}303\Upsilon^{10}\delta^8\kappa^{12} - 149\Upsilon^{10}\delta^6\kappa^{14} - 160{,}104\Upsilon^8\delta^{10}\kappa^{12} + 67{,}632\Upsilon^8\delta^8\kappa^{14} + 28{,}398\Upsilon^6\delta^{12}\kappa^{12} \\
& - 67{,}626\Upsilon^6\delta^{10}\kappa^{14} + 7{,}286\Upsilon^6\delta^8\kappa^{16} + 4{,}958\Upsilon^4\delta^{12}\kappa^{14} - 5{,}165\Upsilon^4\delta^{10}\kappa^{16} + 138\Upsilon^2\delta^{12}\kappa^{16} \\
& + 18{,}924\Upsilon^{11}\delta^8\kappa^{10} - 2{,}467\Upsilon^{11}\delta^6\kappa^{12} - 115{,}479\Upsilon^9\delta^{10}\kappa^{10} + 123{,}888\Upsilon^9\delta^8\kappa^{12} - 145\Upsilon^9\delta^6\kappa^{14} \\
& - 217{,}620\Upsilon^7\delta^{10}\kappa^{12} + 103{,}863\Upsilon^7\delta^8\kappa^{14} + 18{,}196\Upsilon^5\delta^{12}\kappa^{12} - 56{,}490\Upsilon^5\delta^{10}\kappa^{14} + 4{,}068\Upsilon^5\delta^8\kappa^{16} \\
& + 1{,}462\Upsilon^3\delta^{12}\kappa^{14} - 2{,}919\Upsilon^3\delta^{10}\kappa^{16} + 2{,}300\Upsilon^{12}\delta^8\kappa^8 - 486\Upsilon^{12}\delta^6\kappa^{10} + 90{,}884\Upsilon^{10}\delta^8\kappa^{10} \\
& - 15{,}518\Upsilon^{10}\delta^6\kappa^{12} - 229{,}440\Upsilon^8\delta^{10}\kappa^{10} + 260{,}067\Upsilon^8\delta^8\kappa^{12} + 1{,}176\Upsilon^8\delta^6\kappa^{14} \\
& - 206{,}628\Upsilon^6\delta^{10}\kappa^{12} + 115{,}487\Upsilon^6\delta^8\kappa^{14} + 6{,}308\Upsilon^4\delta^{12}\kappa^{12} - 35{,}085\Upsilon^4\delta^{10}\kappa^{14} \\
& + 926\Upsilon^4\delta^8\kappa^{16} + 198\Upsilon^2\delta^{12}\kappa^{14} - 1{,}077\Upsilon^2\delta^{10}\kappa^{16} + 24{,}612\Upsilon^{11}\delta^8\kappa^8 - 5{,}577\Upsilon^{11}\delta^6\kappa^{10} \\
& + 257{,}809\Upsilon^9\delta^8\kappa^{10} - 56{,}680\Upsilon^9\delta^6\kappa^{12} - 301{,}440\Upsilon^7\delta^{10}\kappa^{10} + 380{,}928\Upsilon^7\delta^8\kappa^{12} \\
& + 5{,}058\Upsilon^7\delta^6\kappa^{14} - 137{,}412\Upsilon^5\delta^{10}\kappa^{12} + 93{,}105\Upsilon^5\delta^8\kappa^{14} + 952\Upsilon^3\delta^{12}\kappa^{12} \\
& - 15{,}237\Upsilon^3\delta^{10}\kappa^{14} - 376\Upsilon^3\delta^8\kappa^{16} - 187\Upsilon\delta^{10}\kappa^{16} - 1{,}017\Upsilon^{12}\delta^6\kappa^8 + 116{,}806\Upsilon^{10}\delta^8\kappa^8 \\
& - 29{,}253\Upsilon^{10}\delta^6\kappa^{10} - 15\Upsilon^{10}\delta^4\kappa^{12} + 476{,}667\Upsilon^8\delta^8\kappa^{10} - 134{,}289\Upsilon^8\delta^6\kappa^{12} \\
& - 263{,}523\Upsilon^6\delta^{10}\kappa^{10} + 396{,}168\Upsilon^6\delta^8\kappa^{12} + 10{,}056\Upsilon^6\delta^6\kappa^{14} - 62{,}940\Upsilon^4\delta^{10}\kappa^{12} \\
& + 52{,}963\Upsilon^4\delta^8\kappa^{14} + 18\Upsilon^2\delta^{12}\kappa^{12} - 4{,}041\Upsilon^2\delta^{10}\kappa^{14} - 345\Upsilon^2\delta^8\kappa^{16} \\
& - 10{,}000\Upsilon^{11}\delta^6\kappa^8 + 270\Upsilon^{11}\delta^4\kappa^{10} + 323{,}184\Upsilon^9\delta^8\kappa^8 - 92{,}715\Upsilon^9\delta^6\kappa^{10} \\
& - 249\Upsilon^9\delta^4\kappa^{12} + G_2
\end{aligned} \tag{33}
$$

$$
\begin{aligned}
G_2 = {} & 598{,}500\Upsilon^7\delta^8\kappa^{10} - 217{,}218\Upsilon^7\delta^6\kappa^{12} - 150{,}219\Upsilon^5\delta^{10}\kappa^{10} + 290{,}796\Upsilon^5\delta^8\kappa^{12} + 12{,}230\Upsilon^5\delta^6\kappa^{14} - 19{,}032\Upsilon^3\delta^{10}\kappa^{12} \\
& + 19{,}717\Upsilon^3\delta^8\kappa^{14} - 4{,}77\Upsilon\delta^{10}\kappa^{14} - 98\Upsilon\delta^8\kappa^{16} - 2{,}673\Upsilon^{12}\delta^6\kappa^6 + 369\Upsilon^{12}\delta^4\kappa^8 - 44{,}345\Upsilon^{10}\delta^6\kappa^8 + 2{,}955\Upsilon^{10}\delta^4\kappa^{10} \\
& + 576{,}846\Upsilon^8\delta^8\kappa^8 - 198{,}162\Upsilon^8\delta^6\kappa^{10} - 1{,}506\Upsilon^8\delta^4\kappa^{12} + 515{,}908\Upsilon^6\delta^8\kappa^{10} - 244{,}584\Upsilon^6\delta^6\kappa^{12} - 52{,}714\Upsilon^4\delta^{10}\kappa^{10} \\
& + 145{,}788\Upsilon^4\delta^8\kappa^{12} + 9{,}790\Upsilon^4\delta^6\kappa^{14} - 3{,}480\Upsilon^2\delta^{10}\kappa^{12} + 3{,}912\Upsilon^2\delta^8\kappa^{14} - 10\delta^8\kappa^{16} - 27{,}277\Upsilon^{11}\delta^6\kappa^6 \\
& + 3{,}825\Upsilon^{11}\delta^4\kappa^8 - 116{,}716\Upsilon^9\delta^6\kappa^8 + 14{,}106\Upsilon^9\delta^4\kappa^{10} + 694{,}320\Upsilon^7\delta^8\kappa^8 - 301{,}764\Upsilon^7\delta^6\kappa^{10} - 4{,}848\Upsilon^7\delta^4\kappa^{12} \\
& + 302{,}058\Upsilon^5\delta^8\kappa^{10} - 190{,}624\Upsilon^5\delta^6\kappa^{12} - 9{,}906\Upsilon^3\delta^{10}\kappa^{10} + 46{,}302\Upsilon^3\delta^8\kappa^{12} + 5{,}231\Upsilon^3\delta^6\kappa^{14} - 306\Upsilon\delta^{10}\kappa^{12} \\
& + 80\Upsilon\delta^8\kappa^{14} - 459\Upsilon^{12}\delta^4\kappa^6 - 124{,}592\Upsilon^{10}\delta^6\kappa^6 + 19{,}548\Upsilon^{10}\delta^4\kappa^8 - 203{,}232\Upsilon^8\delta^6\kappa^8 + 38{,}820\Upsilon^8\delta^4\kappa^{10} \\
& + 572{,}398\Upsilon^6\delta^8\kappa^8 - 336{,}960\Upsilon^6\delta^6\kappa^{10} - 9{,}558\Upsilon^6\delta^4\kappa^{12} + 117{,}031\Upsilon^4\delta^8\kappa^{10} - 99{,}125\Upsilon^4\delta^6\kappa^{12} - 612\Upsilon^2\delta^{10}\kappa^{10} \\
& + 7{,}833\Upsilon^2\delta^8\kappa^{12} + 1{,}813\Upsilon^2\delta^6\kappa^{14} - 81\delta^8\kappa^{14} - 6{,}903\Upsilon^{11}\delta^4\kappa^6 - 337{,}144\Upsilon^9\delta^6\kappa^6 + 65{,}088\Upsilon^9\delta^4\kappa^8 + 20\Upsilon^9\delta^2\kappa^{10} \\
& - 250{,}224\Upsilon^7\delta^6\kappa^8 + 68{,}152\Upsilon^7\delta^4\kappa^{10} + 322{,}140\Upsilon^5\delta^8\kappa^8 - 279{,}696\Upsilon^5\delta^6\kappa^{10} - 12{,}282\Upsilon^5\delta^4\kappa^{12} + 29{,}720\Upsilon^3\delta^8\kappa^{10} \\
& - 31{,}099\Upsilon^3\delta^6\kappa^{12} + 36\Upsilon\delta^{10}\kappa^{10} + 372\Upsilon\delta^8\kappa^{12} + 371\Upsilon\delta^6\kappa^{14} + 306\Upsilon^{12}\delta^4\kappa^4 - 43{,}683\Upsilon^{10}\delta^4\kappa^6 - 63\Upsilon^{10}\delta^2\kappa^8 \\
& - 603{,}261\Upsilon^8\delta^6\kappa^6 + 155{,}160\Upsilon^8\delta^4\kappa^8 + 198\Upsilon^8\delta^2\kappa^{10} - 233{,}070\Upsilon^6\delta^6\kappa^8 + 79{,}236\Upsilon^6\delta^4\kappa^{10} + 122{,}018\Upsilon^4\delta^8\kappa^8 \\
& - 173{,}280\Upsilon^4\delta^6\kappa^{10} - 10{,}524\Upsilon^4\delta^4\kappa^{12} + 5{,}772\Upsilon^2\delta^8\kappa^{10} - 4{,}082\Upsilon^2\delta^6\kappa^{12} - 27\delta^8\kappa^{12} + 34\delta^6\kappa^{14} + 1{,}908\Upsilon^{11}\delta^4\kappa^4 \\
& - 27\Upsilon^{11}\delta^2\kappa^6 - 157{,}965\Upsilon^9\delta^4\kappa^6 - 397\Upsilon^9\delta^2\kappa^8 - 755{,}457\Upsilon^7\delta^6\kappa^6 + 274{,}062\Upsilon^7\delta^4\kappa^8 + 848\Upsilon^7\delta^2\kappa^{10} \\
& - 178{,}880\Upsilon^5\delta^6\kappa^8 + 60{,}708\Upsilon^5\delta^4\kappa^{10} + 31{,}092\Upsilon^3\delta^8\kappa^8 - 79{,}707\Upsilon^3\delta^6\kappa^{10} - 5{,}976\Upsilon^3\delta^4\kappa^{12} + 1{,}197\Upsilon\delta^8\kappa^{10} \\
& + 488\Upsilon\delta^6\kappa^{12} + 162\Upsilon^{12}\delta^2\kappa^4 + 2{,}991\Upsilon^{10}\delta^4\kappa^4 - 1{,}431\Upsilon^{10}\delta^2\kappa^6 - 367{,}806\Upsilon^8\delta^4\kappa^6 - 990\Upsilon^8\delta^2\kappa^8 \\
& - 685{,}089\Upsilon^6\delta^6\kappa^6 + 362{,}460\Upsilon^6\delta^4\kappa^8 + 2{,}072\Upsilon^6\delta^2\kappa^{10} - 120{,}301\Upsilon^4\delta^6\kappa^8 + 28{,}826\Upsilon^4\delta^4\kappa^{10} \\
& + 5{,}844\Upsilon^2\delta^8\kappa^8 - 26{,}523\Upsilon^2\delta^6\kappa^{10} - 2{,}163\Upsilon^2\delta^4\kappa^{12} + 171\delta^8\kappa^{10} + 169\delta^6\kappa^{12} + 2{,}970\Upsilon^{11}\delta^2\kappa^4 \\
& - 8{,}196\Upsilon^9\delta^4\kappa^4 - 11{,}904\Upsilon^9\delta^2\kappa^6 - 583{,}302\Upsilon^7\delta^4\kappa^6 - 1{,}112\Upsilon^7\delta^2\kappa^8 - 460{,}571\Upsilon^5\delta^6\kappa^6 + 358{,}524\Upsilon^5\delta^4\kappa^8 \\
& + 3{,}192\Upsilon^5\delta^2\kappa^{10} - 67{,}952\Upsilon^3\delta^6\kappa^8 + 6{,}690\Upsilon^3\delta^4\kappa^{10} + 972\Upsilon\delta^8\kappa^8 - 5{,}853\Upsilon\delta^6\kappa^{10} - 453\Upsilon\delta^4\kappa^{12} \\
& + 1{,}080\Upsilon^{12}\delta^2\kappa^2 + 21{,}042\Upsilon^{10}\delta^2\kappa^4 - 45{,}384\Upsilon^8\delta^4\kappa^4 - 47{,}520\Upsilon^8\delta^2\kappa^6 + G_3
\end{aligned} \tag{34}
$$

$$
\begin{aligned}
G_3 = {} & -4\Upsilon^8\kappa^8 - 645{,}240\Upsilon^6\delta^4\kappa^6 - 182\Upsilon^6\delta^2\kappa^8 - 233{,}344\Upsilon^4\delta^6\kappa^6 + 262{,}293\Upsilon^4\delta^4\kappa^8 + 3{,}220\Upsilon^4\delta^2\kappa^{10} \\
& - 2{,}8137\Upsilon^2\delta^6\kappa^8 - 423\Upsilon^2\delta^4\kappa^{10} + 108\delta^8\kappa^8 - 648\delta^6\kappa^{10} - 42\delta^4\kappa^{12} + 12{,}096\Upsilon^{11}\delta^2\kappa^2 + 82{,}826\Upsilon^9\delta^2\kappa^4 \\
& - 18\Upsilon^9\kappa^6 - 96{,}152\Upsilon^7\delta^4\kappa^4 - 114{,}426\Upsilon^7\delta^2\kappa^6 - 32\Upsilon^7\kappa^8 - 498{,}102\Upsilon^5\delta^4\kappa^6 + 966\Upsilon^5\delta^2\kappa^8 \\
& - 89{,}366\Upsilon^3\delta^6\kappa^6 + 138{,}345\Upsilon^3\delta^4\kappa^8 + 2{,}128\Upsilon^3\delta^2\kappa^{10} - 7{,}140\Upsilon\delta^6\kappa^8 - 614\Upsilon\delta^4\kappa^{10} + 61{,}722\Upsilon^{10}\delta^2\kappa^2 \\
& + 252\Upsilon^{10}\kappa^4 + 208{,}440\Upsilon^8\delta^2\kappa^4 - 124\Upsilon^8\kappa^6 - 120{,}174\Upsilon^6\delta^4\kappa^4 - 182{,}322\Upsilon^6\delta^2\kappa^6 - 112\Upsilon^6\kappa^8 \\
& - 262{,}005\Upsilon^4\delta^4\kappa^6 + 1{,}148\Upsilon^4\delta^2\kappa^8 - 25{,}059\Upsilon^2\delta^6\kappa^6 + 49{,}968\Upsilon^2\delta^4\kappa^8 + 888\Upsilon^2\delta^2\kappa^{10} - 810\delta^6\kappa^8 \\
& - 102\delta^4\kappa^{10} - 216\Upsilon^{11}\kappa^2 + 189{,}794\Upsilon^9\delta^2\kappa^2 + 2{,}340\Upsilon^9\kappa^4 + 359{,}024\Upsilon^7\delta^2\kappa^4 - 344\Upsilon^7\kappa^6 \\
& - 96{,}072\Upsilon^5\delta^4\kappa^4 - 200{,}340\Upsilon^5\delta^2\kappa^6 - 224\Upsilon^5\kappa^8 - 88{,}251\Upsilon^3\delta^4\kappa^6 + 560\Upsilon^3\delta^2\kappa^8 - 4{,}617\Upsilon\delta^6\kappa^6 \\
& + 11{,}100\Upsilon\delta^4\kappa^8 + 212\Upsilon\delta^2\kappa^{10} - 324\Upsilon^{12} - 2{,}268\Upsilon^{10}\kappa^2 + 391{,}788\Upsilon^8\delta^2\kappa^2 + 9{,}768\Upsilon^8\kappa^4 \\
& + 437{,}864\Upsilon^6\delta^2\kappa^4 - 448\Upsilon^6\kappa^6 - 48{,}826\Upsilon^4\delta^4\kappa^4 - 153{,}684\Upsilon^4\delta^2\kappa^6 - 280\Upsilon^4\kappa^8 \\
& - 1{,}6293\Upsilon^2\delta^4\kappa^6 + 93\Upsilon^2\delta^2\kappa^8 - 414\delta^6\kappa^6 + 1{,}146\delta^4\kappa^8 + 22\delta^2\kappa^{10} - 3{,}564\Upsilon^{11} \\
& - 10{,}818\Upsilon^9\kappa^2 + 572{,}056\Upsilon^7\delta^2\kappa^2 + 24{,}144\Upsilon^7\kappa^4 + 382{,}992\Upsilon^5\delta^2\kappa^4 - 140\Upsilon^5\kappa^6 - 14{,}364\Upsilon^3\delta^4\kappa^4 \\
& - 81{,}315\Upsilon^3\delta^2\kappa^6 - 224\Upsilon^3\kappa^8 - 837\Upsilon\delta^4\kappa^6 - 17\Upsilon\delta^2\kappa^8 - 17{,}964\Upsilon^{10} - 30{,}940\Upsilon^8\kappa^2 \\
& + 605{,}836\Upsilon^6\delta^2\kappa^2 + 39{,}144\Upsilon^6\kappa^4 + 239{,}206\Upsilon^4\delta^2\kappa^4 + 392\Upsilon^4\kappa^6 - 1{,}593\Upsilon^2\delta^4\kappa^4 - 28{,}431\Upsilon^2\delta^2\kappa^6 \\
& - 112\Upsilon^2\kappa^8 + 126\delta^4\kappa^6 - 6\delta^2\kappa^8 - 54{,}864\Upsilon^9 - 58{,}952\Upsilon^7\kappa^2 + 468{,}876\Upsilon^5\delta^2\kappa^2 + 43{,}512\Upsilon^5\kappa^4 \\
& + 104{,}230\Upsilon^3\delta^2\kappa^4 + 616\Upsilon^3\kappa^6 + 268\Upsilon\delta^4\kappa^4 - 5{,}940\Upsilon\delta^2\kappa^6 - 32\Upsilon\kappa^8 - 113{,}080\Upsilon^8 - 78{,}568\Upsilon^6\kappa^2 \\
& + 263{,}144\Upsilon^4\delta^2\kappa^2 + 33{,}600\Upsilon^4\kappa^4 + 30{,}102\Upsilon^2\delta^2\kappa^4 + 416\Upsilon^2\kappa^6 + 72\delta^4\kappa^4 - 564\delta^2\kappa^6 - 4\kappa^8 \\
& - 165{,}704\Upsilon^7 - 74{,}732\Upsilon^5\kappa^2 + 104{,}408\Upsilon^3\delta^2\kappa^2 + 17{,}808\Upsilon^3\kappa^4 + 5{,}174\Upsilon\delta^2\kappa^4 + 142\Upsilon\kappa^6 \\
& - 177{,}016\Upsilon^6 - 50{,}728\Upsilon^4\kappa^2 + 27{,}786\Upsilon^2\delta^2\kappa^2 + 6{,}204\Upsilon^2\kappa^4 + 400\delta^2\kappa^4 + 20\kappa^6 - 138{,}896\Upsilon^5 \\
& - 24{,}080\Upsilon^3\kappa^2 + 4{,}450\Upsilon\delta^2\kappa^2 + 1{,}284\Upsilon\kappa^4 - 79{,}444\Upsilon^4 - 7{,}612\Upsilon^2\kappa^2 + 324\delta^2\kappa^2 \\
& + 120\kappa^4 - 32{,}300\Upsilon^3 - 1{,}442\Upsilon\kappa^2 - 8{,}860\Upsilon^2 - 124\kappa^2 - 1{,}472\Upsilon - 112
\end{aligned} \tag{35}
$$

$$
S_5 = \begin{pmatrix}
90(\Upsilon+1)^3\delta^2k^4 \\
\Upsilon^{10}\delta^6\kappa^{12} - 3\Upsilon^8\delta^8\kappa^{12} + 3\Upsilon^6\delta^{10}\kappa^{12} - \Upsilon^4\delta^{12}\kappa^{12} + 9\Upsilon^9\delta^6\kappa^{12} - 18\Upsilon^7\delta^8\kappa^{12} \\
+9\Upsilon^5\delta^{10}\kappa^{12} + 12\Upsilon^{10}\delta^6\kappa^{10} - 24\Upsilon^8\delta^8\kappa^{10} + 36\Upsilon^8\delta^6\kappa^{12} + 12\Upsilon^6\delta^{10}\kappa^{10} \\
-45\Upsilon^6\delta^8\kappa^{12} + 9\Upsilon^4\delta^{10}\kappa^{12} + 108\Upsilon^9\delta^6\kappa^{10} - 144\Upsilon^7\delta^8\kappa^{10} + 84\Upsilon^7\delta^6\kappa^{12} \\
-60\Upsilon^5\delta^8\kappa^{12} + 3\Upsilon^3\delta^{10}\kappa^{12} + 48\Upsilon^{10}\delta^6\kappa^8 - 48\Upsilon^8\delta^8\kappa^8 + 429\Upsilon^8\delta^6\kappa^{10} \\
-354\Upsilon^6\delta^8\kappa^{10} + 123\Upsilon^6\delta^6\kappa^{12} + 33\Upsilon^4\delta^{10}\kappa^{10} - 42\Upsilon^4\delta^8\kappa^{12} + 432\Upsilon^9\delta^6\kappa^8 \\
-288\Upsilon^7\delta^8\kappa^8 + 987\Upsilon^7\delta^6\kappa^{10} - 456\Upsilon^5\delta^8\kappa^{10} + 111\Upsilon^5\delta^6\kappa^{12} + 9\Upsilon^3\delta^{10}\kappa^{10} \\
-12\Upsilon^3\delta^8\kappa^{12} + 64\Upsilon^{10}\delta^6\kappa^6 - 12\Upsilon^{10}\delta^4\kappa^8 + 1{,}728\Upsilon^8\delta^6\kappa^8 + 9\Upsilon^8\delta^4\kappa^{10} \\
-708\Upsilon^6\delta^8\kappa^8 + 1{,}428\Upsilon^6\delta^6\kappa^{10} - 324\Upsilon^4\delta^8\kappa^{10} + 52\Upsilon^4\delta^6\kappa^{12} + 576\Upsilon^9\delta^6\kappa^6 \\
-126\Upsilon^9\delta^4\kappa^8 + 4{,}026\Upsilon^7\delta^6\kappa^8 + 57\Upsilon^7\delta^4\kappa^{10} - 900\Upsilon^5\delta^8\kappa^8 + 1{,}317\Upsilon^5\delta^6\kappa^{10} \\
-120\Upsilon^3\delta^8\kappa^{10} - 87\Upsilon^{10}\delta^4\kappa^6 + 2{,}343\Upsilon^8\delta^6\kappa^6 - 540\Upsilon^8\delta^4\kappa^8 + 6{,}000\Upsilon^6\delta^6\kappa^8 \\
+162\Upsilon^6\delta^4\kappa^{10} - 618\Upsilon^4\delta^8\kappa^8 + 750\Upsilon^4\delta^6\kappa^{10} - 18\Upsilon^2\delta^8\kappa^{10} - 12\Upsilon^2\delta^6\kappa^{12} \\
-846\Upsilon^9\delta^4\kappa^6 + 5{,}553\Upsilon^7\delta^6\kappa^6 - 1{,}302\Upsilon^7\delta^4\kappa^8 + 5{,}898\Upsilon^5\delta^6\kappa^8 + 264\Upsilon^5\delta^4\kappa^{10} \\
-216\Upsilon^3\delta^8\kappa^8 + 240\Upsilon^3\delta^6\kappa^{10} - 4\Upsilon\delta^6\kappa^{12} - 156\Upsilon^{10}\delta^4\kappa^4 - 3{,}606\Upsilon^8\delta^4\kappa^6 \\
-3\Upsilon^8\delta^2\kappa^8 + 8{,}319\Upsilon^6\delta^6\kappa^6 + 36\Upsilon^5\delta^{10}\kappa^{10} - 2{,}007\Upsilon^6\delta^4\kappa^8 + 3{,}792\Upsilon^4\delta^6\kappa^8 \\
+261\Upsilon^4\delta^4\kappa^{10} - 30\Upsilon^2\delta^8\kappa^8 + 33\Upsilon^2\delta^6\kappa^{10} - 1{,}368\Upsilon^9\delta^4\kappa^4 + 3\Upsilon^9\delta^2\kappa^6 \\
-8{,}841\Upsilon^7\delta^4\kappa^6 - 12\Upsilon^7\delta^2\kappa^8 + 8{,}073\Upsilon^5\delta^6\kappa^6 - 2{,}091\Upsilon^5\delta^4\kappa^8 + 1{,}518\Upsilon^3\delta^6\kappa^8 \\
+153\Upsilon^3\delta^4\kappa^{10} + 45\Upsilon^{10}\delta^2\kappa^4 - 5{,}298\Upsilon^8\delta^4\kappa^4 - 30\Upsilon^8\delta^2\kappa^6 - 15\Upsilon^6\delta^2\kappa^8 \\
-1{,}3725\Upsilon^6\delta^4\kappa^6 + 5{,}030\Upsilon^4\delta^6\kappa^6 - 1{,}476\Upsilon^4\delta^4\kappa^8 + 336\Upsilon^2\delta^6\kappa^8 + 48\Upsilon^2\delta^4\kappa^{10} \\
+474\Upsilon^9\delta^2\kappa^4 - 1{,}1856\Upsilon^7\delta^4\kappa^4 - 279\Upsilon^7\delta^2\kappa^6 - 13{,}953\Upsilon^5\delta^4\kappa^6 + 30\Upsilon\delta^6\kappa^8 \\
+1{,}926\Upsilon^3\delta^6\kappa^6 - 660\Upsilon^3\delta^4\kappa^8 + 6\Upsilon\delta^4\kappa^{10} + 153\Upsilon^{10}\delta^2\kappa^2 + 2{,}181\Upsilon^8\delta^2\kappa^4 \\
-16{,}860\Upsilon^6\delta^4\kappa^4 - 891\Upsilon^6\delta^2\kappa^6 - 9{,}231\Upsilon^4\delta^4\kappa^6 + 15\Upsilon^4\delta^2\kappa^8 + 408\Upsilon^2\delta^6\kappa^6 \\
-147\Upsilon^2\delta^4\kappa^8 + 1{,}335\Upsilon^9\delta^2\kappa^2 + 5{,}799\Upsilon^7\delta^2\kappa^4 - 2\Upsilon^7\kappa^6 - 15{,}780\Upsilon^5\delta^4\kappa^4 \\
-1{,}542\Upsilon^5\delta^2\kappa^6 - 3{,}771\Upsilon^3\delta^4\kappa^6 + 12\Upsilon^3\delta^2\kappa^8 + 36\Upsilon\delta^6\kappa^6 + 3\Upsilon\delta^4\kappa^8 \\
+5{,}169\Upsilon^8\delta^2\kappa^2 + 15\Upsilon^8\kappa^4 + 9{,}891\Upsilon^6\delta^2\kappa^4 - 12\Upsilon^6\kappa^6 - 9{,}714\Upsilon^4\delta^4\kappa^4 \\
+36\Upsilon\delta^6\kappa^6 + 3\Upsilon\delta^4\kappa^8 + 5{,}169\Upsilon^8\delta^2\kappa^2 + 15\Upsilon^8\kappa^4 + 9{,}891\Upsilon^6\delta^2\kappa^4 \\
-12\Upsilon^6\kappa^6 - 9{,}714\Upsilon^4\delta^4\kappa^4 + G_4
\end{pmatrix} \tag{36}
$$

$$
\begin{aligned}
G_4 = {} & -1{,}632\Upsilon^4\delta^2\kappa^6 - 816\Upsilon^2\delta^4\kappa^6 + 3\Upsilon^2\delta^2\kappa^8 + 6\delta^4\kappa^8 - 9\Upsilon^9\kappa^2 - 30\Upsilon^5\kappa^6 - 54\Upsilon^{10} \\
& - 30\Upsilon^3\kappa^6 + 11{,}691\Upsilon^7\delta^2\kappa^2 + 108\Upsilon^7\kappa^4 + 11{,}319\Upsilon^5\delta^2\kappa^4 - 3{,}792\Upsilon^3\delta^4\kappa^4 \\
& - 1{,}095\Upsilon^3\delta^2\kappa^6 - 45\Upsilon\delta^4\kappa^6 - 78\Upsilon^8\kappa^2 + 17{,}094\Upsilon^6\delta^2\kappa^2 + 339\Upsilon^6\kappa^4 + 8{,}799\Upsilon^4\delta^2\kappa^4 \\
& - 40\Upsilon^4\kappa^6 - 852\Upsilon^2\delta^4\kappa^4 - 459\Upsilon^2\delta^2\kappa^6 + 9\delta^4\kappa^6 - 468\Upsilon^9 - 300\Upsilon^7\kappa^2 + 16{,}866\Upsilon^5\delta^2\kappa^2 \\
& + 606\Upsilon^5\kappa^4 + 4{,}581\Upsilon^3\delta^2\kappa^4 - 84\Upsilon\delta^4\kappa^4 - 111\Upsilon\delta^2\kappa^6 - 1{,}821\Upsilon^8 - 672\Upsilon^6\kappa^2 \\
& + 11{,}355\Upsilon^4\delta^2\kappa^2 + 675\Upsilon^4\kappa^4 + 1{,}524\Upsilon^2\delta^2\kappa^4 - 12\Upsilon^2\kappa^6 - 12\delta^2\kappa^6 - 4{,}190\Upsilon^7 \\
& - 966\Upsilon^5\kappa^2 + 5{,}139\Upsilon^3\delta^2\kappa^2 + 480\Upsilon^3\kappa^4 + 291\Upsilon\delta^2\kappa^4 - 2\Upsilon\kappa^6 - 6{,}315\Upsilon^6 \\
& - 924\Upsilon^4\kappa^2 + 1{,}491\Upsilon^2\delta^2\kappa^2 + 213\Upsilon^2\kappa^4 + 24\delta^2\kappa^4 - 6{,}516\Upsilon^5 - 588\Upsilon^3\kappa^2 \\
& + 249\Upsilon\delta^2\kappa^2 + 54\Upsilon\kappa^4 - 4{,}663\Upsilon^4 - 240\Upsilon^2\kappa^2 + 18\delta^2\kappa^2 + 6\kappa^4 - 2{,}286\Upsilon^3 \\
& - 57\Upsilon\kappa^2 - 735\Upsilon^2 - 6\kappa^2 - 140\Upsilon - 12
\end{aligned} \tag{37}
$$

Data Availability Statement

All data, models, and code generated or used during the study appear in the published article.

Acknowledgments

The authors would like to acknowledge the Inspire faculty grant, Grant No. DST/INSPIRE/04/2018/000052, for partial financial support for the project. Sudip Chowdhury would like to acknowledge the MHRD grant received from IIT Delhi during the period of this research work, the IRD Early-Doc Fellowship received from IIT Delhi during the period of this research work, and the Postdoctoral Research Grant received from the University of Glasgow during the period of this research work.

Notation

The following symbols are used in this paper:

c = damping of the SDOF system;
c_u = effective damping of the absorber;
c_v = static damping of the absorber;
k = stiffness of the SDOF system;
k_u = effective stiffness of the absorber;
k_v = static stiffness of the absorber;
m = mass of the SDOF system;
m_u = effective mass of the absorber;
m_v = static mass of the absorber;
m_z = Amplifier's mass;
P = external/Applied force;
P_a = harvested power;
R_v = electrical resistance;
S_0 = spectral density;
W_s = the dynamic response of the SDOF system;
W_u = The dynamic response of the absorber;
W_v = the voltage of the piezoelectric stack;
β = electromechanical coupling of the harvester;
δ = nondimensional time constant;
ε = natural frequency of SDOF system;
ζ = damping ratio of SDOF system;
η = excitation frequency ratio;
κ = nondimensional electromechanical coupling coefficient;
ν = natural frequency of absorber;
v_s = the deflection of SDOF system;
v_u = the deflection of absorber;
ξ = damping ratio of absorber;
$\Sigma^2_{W_s}$ = the variance of the dynamic response of the structure;
τ = electrical capacitance;
Υ = effective mass ratio of absorber;
Υ_D = total mass ratio of each absorber;
Υ_v = absorber mass ratio;
Υ_z = amplifier mass ratio;
ϕ = amplifier/inertial angle;
χ = frequency ratio of absorber; and
ω = excitation frequency.

References

Adhikari, S., and A. Banerjee. 2022. "Enhanced low-frequency vibration energy harvesting with inertial amplifiers." *J. Intell. Mater. Syst. Struct.* 33 (6): 822–838. https://doi.org/10.1177/1045389X211032281.

Adhikari, S., M. Friswell, and D. Inman. 2009. "Piezoelectric energy harvesting from broadband random vibrations." *Smart Mater. Struct.* 18 (11): 115005. https://doi.org/10.1088/0964-1726/18/11/115005.

Ali, S., M. Friswell, and S. Adhikari. 2010. "Piezoelectric energy harvesting with parametric uncertainty." *Smart Mater. Struct.* 19 (10): 105010. https://doi.org/10.1088/0964-1726/19/10/105010.

Ali, S., M. Friswell, and S. Adhikari. 2011. "Analysis of energy harvesters for highway bridges." *J. Intell. Mater. Syst. Struct.* 22 (16): 1929–1938. https://doi.org/10.1177/1045389X11417650.

Ali, S. F., and S. Adhikari. 2013. "Energy harvesting dynamic vibration absorbers." *J. Appl. Mech.* 80 (4): 041004. https://doi.org/10.1115/1.4007967.

Brennan, M., B. Tang, G. P. Melo, and V. Lopes Jr. 2014. "An investigation into the simultaneous use of a resonator as an energy harvester and a vibration absorber." *J. Sound Vib.* 333 (5): 1331–1343. https://doi.org/10.1016/j.jsv.2013.10.035.

Caracoglia, L. 2024. "Improving output power of a torsional-flutter harvester in stochastic thunderstorms by Duffing-van der Pol restoring torque." *ASCE-ASME J Risk Uncertainty Eng. Syst. Part B Mech. Eng.* 10 (4): 041204. https://doi.org/10.1115/1.4065532.

Chen, M. Z., and Y. Hu. 2019. *Inerter and its application in vibration control systems*. New York: Springer.

Chen, X., Y. Leng, F. Sun, X. Su, S. Sun, and J. Xu. 2023. "A novel triple-magnet magnetic suspension dynamic vibration absorber." *J. Sound Vib.* 546 (Apr): 117483. https://doi.org/10.1016/j.jsv.2022.117483.

Chowdhury, S., and S. Adhikari. 2024. "Nonlinear inertial amplifier liquid column dampers." *Appl. Math. Modell.* 140 (Apr): 15875.

Chowdhury, S., and A. Banerjee. 2024. "The impacting vibration absorbers." *Appl. Math. Modell.* 127 (Sep): 454–505. https://doi.org/10.1016/j.apm.2023.12.007.

Chowdhury, S., A. Banerjee, and S. Adhikari. 2023. "The optimum inertial amplifier tuned mass dampers for nonlinear dynamic systems." *Int. J. Appl. Mech.* 15 (02): 2350009. https://doi.org/10.1142/S1758825123500096.

Chowdhury, S., A. Banerjee, and S. Adhikari. 2024a. "A critical review on inertially-amplified passive vibration control devices." *Arch. Comput. Methods Eng.* 31 (4): 2139–2175. https://doi.org/10.1007/s11831-023-10040-z.

Chowdhury, S., A. Banerjee, and S. Adhikari. 2024b. "Enhancing seismic resilience of structures through optimally designed nonlinear negative stiffness base isolators: Exact closed-form expressions." *Nonlinear Dyn.* 112 (18): 15833–15856. https://doi.org/10.1007/s11071-024-09892-2.

Chowdhury, S., A. Banerjee, and S. Adhikari. 2024c. "From impact to control: Inertially amplified friction bearings." *ASCE-ASME J. Risk Uncertainty Eng. Syst. Part A: Civ. Eng.* 10 (4): 04024071. https://doi.org/10.1061/AJRUA6.RUENG-1407.

Chowdhury, S., A. Banerjee, and S. Adhikari. 2024d. "The optimum inerter-based additional viscoelastic mass dampers for dynamic response mitigation of structures." *Mech. Based Des. Struct. Mach.* 52 (7): 3775–3798. https://doi.org/10.1080/15397734.2023.2209460.

Chowdhury, S., and R. Debbarma. 2025. "Presenting the potential of optimum torsionally coupled base isolators for vibration control of torsionally coupled structures: Exact closed-form expressions." *J. Struct. Des. Constr. Pract.* 30 (2): 04024111. https://doi.org/10.1061/JSDCCC.SCENG-1616.

Den Hartog, J. 1956. *Mechanical vibrations*. 4th ed. New York: McGraw-Hill.

dos Santos, K. R. 2023. "Electrical response estimation of vibratory energy harvesters via Hilbert transform based stochastic averaging." *ASCE-ASME J. Risk Uncertainty Eng. Syst. Part B: Mech. Eng.* 9 (4): 041201. https://doi.org/10.1115/1.4062704.

Frandsen, N. M., O. R. Bilal, J. S. Jensen, and M. I. Hussein. 2016. "Inertial amplification of continuous structures: Large band gaps from small masses." *J. Appl. Phys.* 119 (12): 124902. https://doi.org/10.1063/1.4944429.

Giaralis, A. 2021. "An inerter-based dynamic vibration absorber with concurrently enhanced energy harvesting and motion control performances under broadband stochastic excitation via inertance amplification." *ASCE-ASME J. Risk Uncertainty Eng. Syst. Part B: Mech. Eng.* 7 (1): 010909. https://doi.org/10.1115/1.4049213.

Huang, S.-C., L.-H. Nguyen, J.-W. Liang, and Y.-M. Huang. 2018. "Design and analysis of a collocated periodic vibration absorber-harvester." *Int. J. Mech. Sci.* 148 (Mar): 337–351. https://doi.org/10.1016/j.ijmecsci.2018.09.009.

Huo, Z., H. Ding, and Z. Shu. 2023. "Optimal design of tuned inerter eddy current damper." *Soil Dyn. Earthquake Eng.* 171 (Jun): 107942. https://doi.org/10.1016/j.soildyn.2023.107942.

Iwata, Y. 1982. "On the construction of the dynamic vibration absorbers." *Jpn. Soc. Mech. Eng.* 820 (8): 150–152.

Kakou, P., and O. Barry. 2021. "Simultaneous vibration reduction and energy harvesting of a nonlinear oscillator using a nonlinear electromagnetic vibration absorber-inerter." *Mech. Syst. Signal Process.* 156 (Jul): 107607. https://doi.org/10.1016/j.ymssp.2021.107607.

Kang, X., X. Wang, A. Zhang, and G. Xia. 2024. "Low frequency vibration energy harvesting of piezoelectric vibration systems with an adjustable device and inertial amplifier device." *J. Vib. Eng. Technol.* 12: 1–25. https://doi.org/10.1007/s42417-024-01442-9.

Kiureghian, A. D., and A. Neuenhofer. 1992. "Response spectrum method for multi-support seismic excitations." *Earthquake Eng. Struct. Dyn.* 21 (8): 713–740. https://doi.org/10.1002/eqe.4290210805.

Krenk, S. 2005. "Frequency analysis of the tuned mass damper." *J. Appl. Mech.* 72 (6): 936–942. https://doi.org/10.1115/1.2062867.

Loong, C. N., E. G. Dimitrakopoulos, and C.-C. Chang. 2023. "Nonlinear electromagnetic energy harvester–structure system under seismic excitation: Vibration mitigation and energy scavenging." *J. Eng. Mech.* 149 (9): 04023058. https://doi.org/10.1061/JENMDT.EMENG-7107.

Madhav, C., and S. F. Ali. 2016. "Harvesting energy from vibration absorber under random excitations." *IFAC-PapersOnLine* 49 (1): 807–812. https://doi.org/10.1016/j.ifacol.2016.03.156.

Nishihara, O., and T. Asami. 2002. "Closed-form solutions to the exact optimizations of dynamic vibration absorbers (minimizations of the maximum amplitude magnification factors)." *J. Vib. Acoust.* 124 (4): 576–582. https://doi.org/10.1115/1.1500335.

Ormondroyd, J., and J. Den Hartog. 1928. "The theory of the dynamic vibration absorber." *J. Fluids Eng.* 49–50 (2): 021007. https://doi.org/10.1115/1.4058553.

Raj, P. R., and B. Santhosh. 2019. "Parametric study and optimization of linear and nonlinear vibration absorbers combined with piezoelectric energy harvester." *Int. J. Mech. Sci.* 152 (Apr): 268–279. https://doi.org/10.1016/j.ijmecsci.2018.12.053.

Rajarathinam, M., and S. F. Ali. 2021. "Parametric uncertainty and random excitation in energy harvesting dynamic vibration absorber." *ASCE-ASME J. Risk Uncertainty Eng. Syst. Part B: Mech. Eng.* 7 (1): 010905. https://doi.org/10.1115/1.4049211.

Roberts, J. B., and P. D. Spanos. 2003. *Random vibration and statistical linearization*. Chelmsford, UK: Courier Corporation.

Shen, Y., H. Peng, X. Li, and S. Yang. 2017. "Analytically optimal parameters of dynamic vibration absorber with negative stiffness." *Mech. Syst. Signal Process.* 85 (Apr): 193–203. https://doi.org/10.1016/j.ymssp.2016.08.018.

Smith, M. C. 2002. "Synthesis of mechanical networks: The inerter." *IEEE Trans. Autom. Control* 47 (10): 1648–1662. https://doi.org/10.1109/TAC.2002.803532.

Su, N., J. Bian, Z. Chen, and Y. Xia. 2023. "A novel lever-type inerter-based vibration absorber." *Int. J. Mech. Sci.* 254 (Jun): 108440. https://doi.org/10.1016/j.ijmecsci.2023.108440.

Su, N., Z. Chen, Y. Xia, and J. Bian. 2024. "Hybrid analytical h-norm optimization approach for dynamic vibration absorbers." *Int. J. Mech. Sci.* 264 (Sep): 108796. https://doi.org/10.1016/j.ijmecsci.2023.108796.

Wang, X., T. He, Y. Shen, Y. Shan, and X. Liu. 2019. "Parameters optimization and performance evaluation for the novel inerter-based dynamic vibration absorbers with negative stiffness." *J. Sound Vib.* 463 (Aug): 114941. https://doi.org/10.1016/j.jsv.2019.114941.

Warburton, G. B. 1982. "Optimum absorber parameters for various combinations of response and excitation parameters." *Earthquake Eng. Struct. Dyn.* 10 (3): 381–401. https://doi.org/10.1002/eqe.4290100304.

Yilmaz, C., G. M. Hulbert, and N. Kikuchi. 2007. "Phononic band gaps induced by inertial amplification in periodic media." *Phys. Rev. B: Condens. Matter Mater. Phys.* 76 (5): 054309. https://doi.org/10.1103/PhysRevB.76.054309.

Yu, Y., X.-X. Jia, H. Ouyang, Y. Du, and Y. Peng. 2024. "Dynamic properties investigation of an acoustic black hole beam with dynamic vibration absorber based on analytical method." *J. Sound Vib.* 570 (Aug): 118053. https://doi.org/10.1016/j.jsv.2023.118053.

Zilletti, M., S. J. Elliott, and E. Rustighi. 2012. "Optimisation of dynamic vibration absorbers to minimise kinetic energy and maximise internal power dissipation." *J. Sound Vib.* 331 (18): 4093–4100. https://doi.org/10.1016/j.jsv.2012.04.023.